Heliyon 10 (2024) e24356

Contents lists available at ScienceDirect

Heliyon

journal homepage: www.cell.com/heliyon

Research article

Transcriptomics analysis reveals distinct mechanism of breast cancer stem cells regulation in mammospheres from MCF-7 and T47D cells

Adam Hermawan [a,b,c,*], Herwandhani Putri [b], Nurul Fatimah [c], Heri Himawan Prasetio [a]

[a] *Laboratory of Macromolecular Engineering, Department of Pharmaceutical Chemistry, Faculty of Pharmacy, Universitas Gadjah Mada Sekip Utara II, 55281, Yogyakarta, Indonesia*
[b] *Cancer Chemoprevention Research Center, Faculty of Pharmacy, Universitas Gadjah Mada Sekip Utara II, 55281, Yogyakarta, Indonesia*
[c] *Laboratory of Advanced Pharmaceutical Sciences. APSLC Building, Faculty of Pharmacy, Universitas Gadjah Mada Sekip Utara II, 55281, Yogyakarta, Indonesia*

ARTICLE INFO

Keywords:
Breast cancer stem cells
Transcriptomics profile
Bioinformatics
Targeted therapy

ABSTRACT

Luminal A breast cancer, constituting 70 % of breast cancer cases, presents a challenge due to the development of resistance and recurrence caused by breast cancer stem cells (BCSC). Luminal breast tumors are characterized by *TP53* expression, a tumor suppressor gene involved in maintaining stem cell attributes in cancer. Although a previous study successfully developed mammospheres (MS) from MCF-7 (with wild-type *TP53*) and T47D (with mutant *TP53*) luminal breast cancer cells for BCSC enrichment, their transcriptomic profiles remain unclear. We aimed to elucidate the transcriptomic disparities between MS of MCF-7 and T47D cells using bioinformatics analyses of differentially expressed genes (DEGs), including the KEGG pathway, Gene Ontology (GO), drug-gene association, disease-gene association, Gene Set Enrichment Analysis (GSEA), DNA methylation analysis, correlation analysis of DEGs with immune cell infiltration, and association analysis of genes and small-molecule compounds via the Connectivity Map (CMap). Upregulated DEGs were enriched in metabolism-related KEGG pathways, whereas downregulated DEGs were enriched in the MAPK signaling pathway. Drug-gene association analysis revealed that both upregulated and downregulated DEGs were associated with fostamatinib. The KEGG pathway GSEA results indicated that the DEGs were enriched for oxidative phosphorylation, whereas the downregulated DEGs were negatively enriched for the p53 signaling pathway. Examination of DNA methylation revealed a noticeable disparity in the expression patterns of the *PKM2, ERO1L, SLC6A6, EPAS1, APLP2, RPL10L*, and *NEDD4* genes when comparing cohorts with low- and high-risk breast cancer. Furthermore, a significant positive correlation was identified between *SLC6A6* expression and macrophage presence, as well as *MSN*, and *AKR1B1* expression and neutrophil and dentritic cell infiltration. CMap analysis unveiled SA-83851 as a potential candidate to counteract the effects of DEGs, specifically in cells harbouring mutant *TP53*. Further research, including *in vitro* and *in vivo* validations, is warranted to develop drugs targeting BCSCs.

* Corresponding author. Laboratory of Macromolecular Engineering, Department of Pharmaceutical Chemistry, Faculty of Pharmacy, Universitas Gadjah Mada, Sekip Utara II, 55281, Yogyakarta, Indonesia.
E-mail address: adam_apt@ugm.ac.id (A. Hermawan).

https://doi.org/10.1016/j.heliyon.2024.e24356
Received 8 April 2023; Received in revised form 4 December 2023; Accepted 8 January 2024
Available online 12 January 2024

1. Introduction

Breast cancer is the leading cause of cancer-related deaths among women worldwide [1]. The luminal A breast cancer subtype, characterized by the expression of the estrogen and progesterone receptors, accounts for 70 % of all breast cancer cases [2]. While antiestrogen treatment is an available option for managing the luminal subtype of breast cancer, the long-term use of this therapy may result in resistance and recurrence caused by a small population of breast cancer cells, namely, breast cancer stem cells (BCSC) [3]. Therefore, the development of BCSC-targeted breast cancer therapies is expected to improve the success rate in treating this luminal breast cancer subtype [4].

Luminal breast cancer cells exhibit distinct characteristics, including the expression of *TP53*, a tumor suppressor gene that plays a role in maintaining stem cell properties in cancer [5]. Previous studies have demonstrated that *TP53* serves as a potential target gene for several compounds, including naringenin and hesperidin, for the inhibition of BCSC [6–8]. However, studies using mutant/deficient *TP53* cells have not yet been conducted. MCF-7 and T47D are members of the luminal A breast cancer subtype that carry wild-type *TP53* and mutant *TP53*, respectively [9].

A genomic study revealed the transcriptomic profiles of different subtypes of breast cancer in various cell lines, such as luminal (MCF-7 and T47D), HER2+ (BT474), and triple-negative breast cancer (e.g., MDA-MB 231 and MDA-MB 436) [10]; however, these analyses were conducted in monolayer cells. In another study, MS were successfully generated from MCF-7 and T47D cells, with subsequent transcriptomic analysis conducted on the MS, albeit without a comparative examination between MCF-7 and T47D cells [11]. Moreover, Verigos et al. (2021) explored the key genes involved in BCSC regulation using MS from MCF-7 cells [12]; however, no information is available on their transcriptomic profiling. Therefore, investigating the mechanisms of BCSCs in two luminal breast cancer cell lines with distinct characteristics, particularly *TP53* status, holds the potential to shed light on the mechanism of the disparities in BCSC regulation and aid in establishing optimal target therapies for BCSC-targeted anticancer treatments.

The aim of this study was to determine the transcriptomic profile of MS from MCF-7 and T47D breast cancer cells during BCSC maintenance using genomic and bioinformatics techniques. These findings are poised to contribute to existing knowledge and accelerate the advancement of anticancer drugs tailored to specifically target BCSCs in luminal breast cancer, particularly within the context of both wild-type and mutant *TP53*.

2. Materials and methods

2.1. Cell cultures

MCF-7 and T47D cells (ATCC, Manassas, VA, USA) were cultured in Dulbecco's modified Eagle's medium (DMEM) containing 20 % fetal bovine serum (FBS) and 10 % FBS, respectively, as well as penicillin–streptomycin, in a 5 % CO_2 incubator at 37 °C. The generate mammospheres (MS), a previously described method [6]. Briefly, the cells (40,000 cells/mL) were cultured on a 50 mg/mL polyHEMA-coated tissue culture dish in mammosphere growth medium containing DMEM, epidermal growth factor (EGF; 10 ng/mL; Sino Biological, Beijing, China), B27 supplement (10 ng/mL; Gibco, Billings, MT, USA), insulin (5 μg/mL; Gibco), and penicillin–streptomycin (1.5 %; Sigma-Aldrich, St. Louis, MO, USA) The MS were cultured for 96 h prior to RNA isolation. The quality of RNA was assessed by RIN >6 and A260/A280 ~ 2.

2.2. Real-time quantitative reverse transcription-polymerase chain reaction (qRT-PCR)

Real-time qRT-PCR was performed to analyze the stem cell characteristics of the MS. BCSC markers, including *SOX2, CD133, ALDH1, OCT4,* and *NANOG* were analyzed using selected primers (Supplementary Table 1). Total mRNA was extracted using RNeasy kits (QIAGEN, Hilden, Germany) following the manufacturer's instructions. The SensiFAST™ cDNA Synthesis Kit was used to generate cDNA (Meridian Bioscience Inc., Cincinnati, OH, USA) and the SensiFAST™ Probe No-ROX Kit (Meridan Biocience) was employed for PCR quantification. GAPDH served as the housekeeping gene. Comparative threshold cycle (ΔΔCT) analysis was performed to examine the findings [13]. Statistical analysis of the real-time qRT-PCR results was performed using Student's *t* test. Statistical significance symbols are described in the tables/figures in which the values are presented.

2.3. Next-generation sequencing

The MS were cultured for 96 h prior to RNA isolation. RNA was extracted using the RNeasy kit (QIAGEN) in accordance with the manufacturer's instructions. The quality of RNA was assessed by RIN >6 and A260/A280 ~ 2. One biological replicate was prepared. Subsequently, total RNA was prepared for next-generation sequencing using the Illumina HiSeq4000 with HiSeq-X sequencing technology (Illumina, San Diengo, CA, USA). This process involved mRNA enrichment, double-stranded cDNA synthesis, end repair, the addition of an A overhang and an A adaptor, fragment selection, PCR amplification, library quality testing, and library quality checking. The quality of the cleaned reads was assessed using FastQC version 0.11.9 (https://github.com/s-andrews/FastQC), and reports were generated using MultiQC version 1.1 (https://multiqc.info). Kallisto (version 0.461), a pseudo-alignment method, was employed to quantify the transcripts using the human genome as a reference (GRCh38.p14) [14]. Statistical significance was set at $p <$ 0 for the analysis of differentially expressed genes (DEGs) using EdgeR version 3.34.0 [15].

2.4. KEGG pathway and Gene Ontology (GO) enrichment analyses

KEGG pathway and GO enrichment analyses were conducted using ShinyGO 0.76.2 (http://bioinformatics.sdstate.edu/go/), following established protocols [16]. Briefly, DEGs were entered into ShinyGO as a gene list for *Homo sapiens*, with a false discovery rate (FDR) cutoff of 0.05, and pathways to show the top 20 with a minimum size of two and a maximum size of 2,000, based on the default settings of ShinyGO.

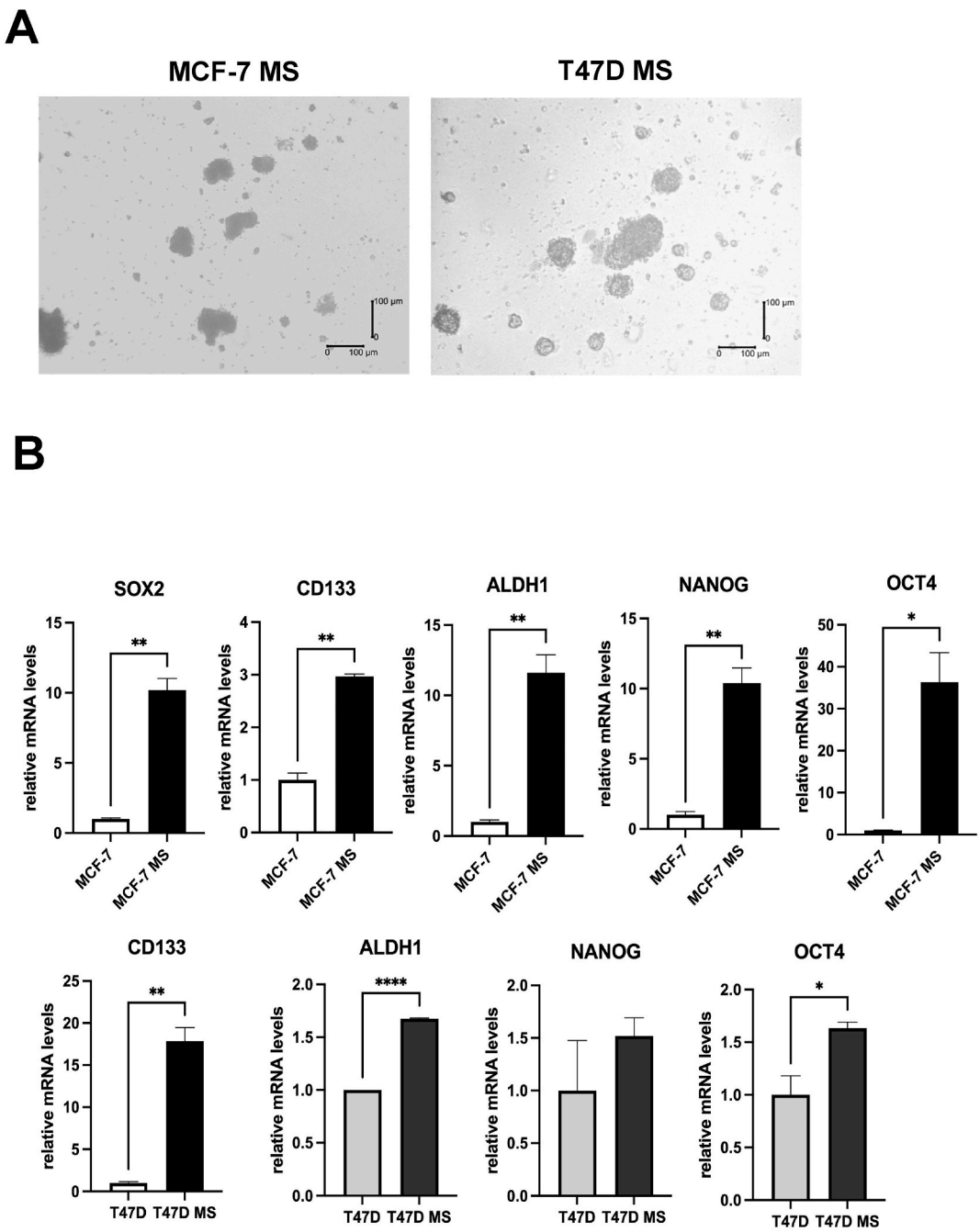

Fig. 1. (A). The morphology of the MS from MCF-7 and T47D cells. (B). The characterization of the BCSCs properties in the MS from MCF-7 cells. The gene expression of *SOX2*, *CD133, ALDH1, NANOG*, and *OCT4* were measured by real-time qRT-PCR. *GAPDH* was used as the internal control. Gene expression was shown as a comparative threshold cycle (ΔΔCT) relative to respective monolayer cells. The results were presented as mean ± SD (n = 3). Statistical analysis was performed using Student's *t* test. *, **, and **** indicate $p < 0.05$, 0.01, and 0.0001, respectively. BCSCs: breast cancer stem cells; qRT-PCR: quantitative reverse transcription polymerase chain reaction; SD: standard deviation.

2.5. Drug-gene and disease-gene association analyses

Drug-gene association analysis was conducted with the Over-Representation Analysis (ORA) of WebGestalt [17] using the DrugBank database. Disease-gene association analysis was conducted using the ORA of WebGestalt [17] with reference to the DISGENET database. The threshold was defined as an FDR of <0.05.

2.6. Gene Set Enrichment Analysis (GSEA)

GSEA was conducted using WebGestalt, incorporating the functional databases of GO non-redundant and KEGG pathway [17]. The threshold was defined as a FDR of <0.05. The normalized enrichment score (NES) indicated the level of enrichment. A notable positive NES signified that the gene set members tended to be positioned towards the top of the transcriptome data rankings. Conversely, a substantial negative NES indicated the opposite trend.

2.7. DNA methylation analysis

To investigate the expression and prognostic trends associated with the methylation of individual CpG sites within the genes *PKM, NDRG1, LDHA, ERO1A, IGFBP3, ACTG1, RPL13A, SLC6A6, EPAS1*, *NCOA3*, *APLP2, MSN, RPL10L, GSTP1, CXCL3, NEDD4, RPL23P8, AKR1B1, SDCBP,* and *ST13*, we employed the MethSurv tool (https://biit.cs.ut.ee/methsurv/). The MethSurv tool facilitates the survival analysis of CpG sites situated either within or in close proximity to a target gene [18]. DNA methylation values were represented as beta values ranging from 0 to 1, calculated using formula $M/(M + U + 100)$, where M and U are the methylated and unmethylated intensity values, respectively, according to the methodology outlined in a previous study [19].

2.8. Correlation analysis of immune cell infiltration with DEGs

The correlation between the top 10 upregulated and top 10 downregulated DEGs and immune cell infiltration was computed using the TIMER 2.0 database (http://timer.cistrome.org/), which offers four modules for examining the correlations between immune infiltrates and genetic or clinical characteristics. It includes modules for investigating cancer-related associations within The Cancer Genome Atlas (TCGA) cohort [20]. Correlation analyses were conducted using Spearman's correlation coefficients, with correlation strength categorized as very weak (0.00–0.19), weak (0.20–0.39), moderate (0.40–0.69), strong (0.70–0.89), and very strong (0.90–1.0). A negative score indicated an inverse correlation, whereas a positive value indicated a direct association. Statistical significance was set at $p < 0.05$ [21].

2.9. Association analysis of genes and small molecule compounds using the Connectivity Map (CMap)

The top 150 DEGs, both upregulated and downregulated, were submitted to The "Connectivity Map" (https://clue.io/about), a valuable tool for identifying associations between small molecules that exhibit a common mode of action, chemicals and physiological

Table 1
Top 10 upregulated and downregulated genes.

No	Gene Symbol	Description	log2 FC
Upregulation			
1	*PKM*	pyruvate kinase M1/2 (PKM), transcript variant 1	17.21035327
2	*NDRG1*	N-myc downstream regulated 1 (NDRG1), transcript variant 2	17.04141021
3	*LDHA*	lactate dehydrogenase A (LDHA), transcript variant 1	16.17491095
4	*ERO1A*	endoplasmic reticulum oxidoreductase 1 alpha (ERO1A), transcript variant 2	15.7880014
5	*IGFBP3*	insulin like growth factor binding protein 3 (IGFBP3), transcript variant 2	15.74685779
6	*ACTG1*	actin gamma 1 (ACTG1), transcript variant 2	15.73094347
7	*RPL13A*	ribosomal protein L13a (RPL13A), transcript variant 1	15.59983842
8	*SLC6A6*	solute carrier family 6 member 6 (SLC6A6), transcript variant 1	15.23804852
9	*EPAS1*	endothelial PAS domain protein 1 (EPAS1)	15.1565463
10	*NCOA3*	nuclear receptor coactivator 3 (NCOA3), transcript variant 1	15.09550225
Downregulation			
No	Gene Symbol	Description	log2 FC
1	*APLP2*	amyloid beta precursor like protein 2 (APLP2), transcript variant 28	−14.82759112
2	*MSN*	moesin (MSN), transcript variant X1	−14.62380513
3	*RPL10L*	ribosomal protein L10 like (RPL10L)	−14.60905948
4	*GSTP1*	glutathione S-transferase pi 1 (GSTP1)	−14.34087419
5	*CXCL3*	C-X-C motif chemokine ligand 3 (CXCL3)	−14.3184444
6	*NEDD4*	NEDD4 E3 ubiquitin protein ligase (NEDD4), transcript variant X3	−14.19014372
7	*RPL23P8*	ribosomal protein L23 pseudogene 8 (RPL23P8), non-coding RNA	−14.07946952
8	*AKR1B1*	aldo-keto reductase family 1 member B (AKR1B1), transcript variant 1	−14.03208017
9	*SDCBP*	syndecan binding protein (SDCBP), transcript variant 5	−14.00215653
10	*ST13*	ST13 Hsp70 interacting protein (ST13), transcript variant 2	−13.88599408

processes, as well as diseases and medications [22,23]. The drugs/molecules were ranked according to their *p*-values, with selection based on the DEGs in BCSCs derived from the MCF-7 and T47D cell lines, compared with the CMap database.

3. Results

3.1. Mammosphere formation and characterization and next-generation sequencing

We successfully generated MS from the MCF-7 and T47D cells (Fig. 1A). Characterization of the formed MS was performed through real-time qRT-PCR, revealing an upregulation of the BCSC markers in the MS from both cell lines (Fig. 1B). Specifically, in MCF-7 MS,

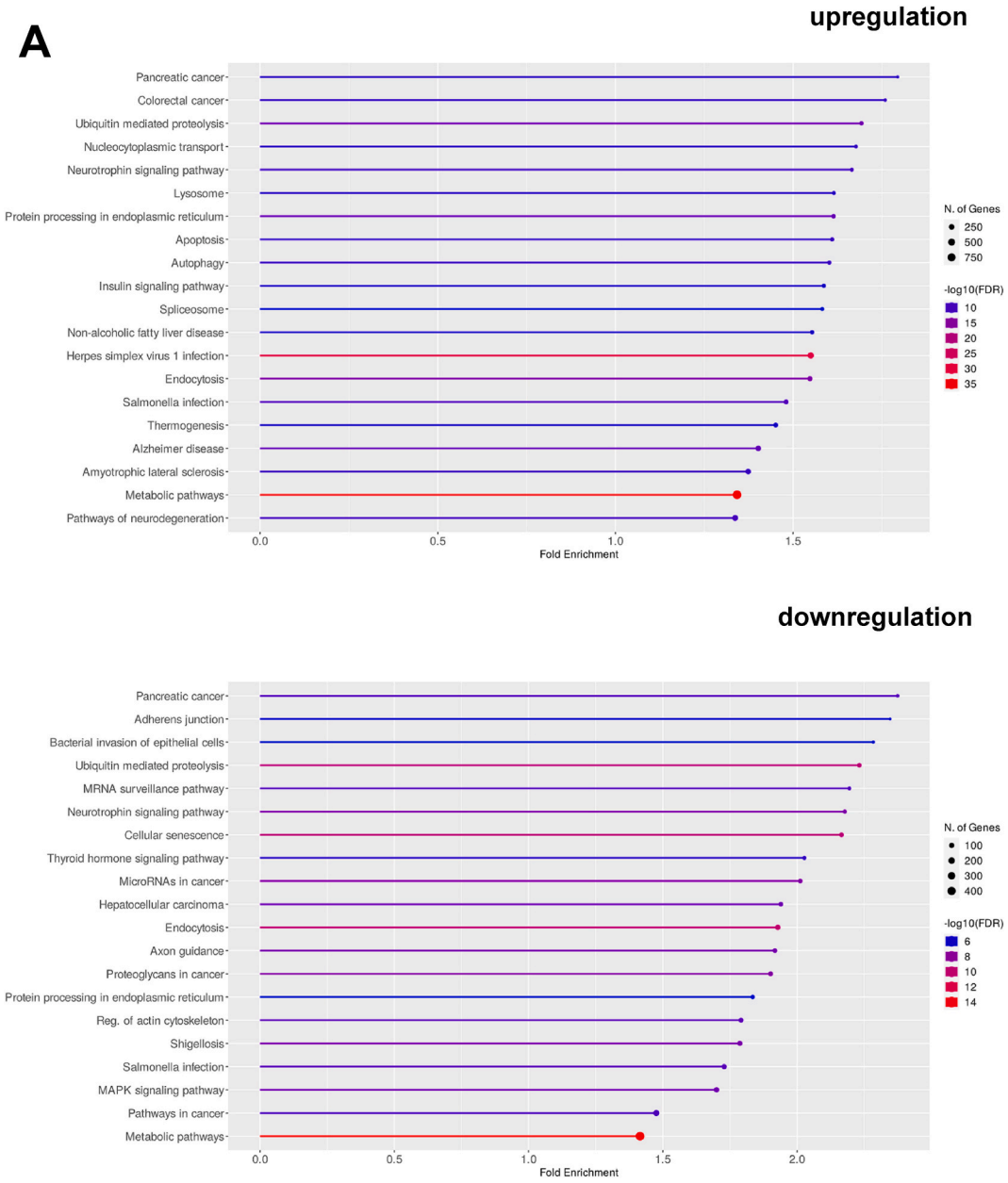

Fig. 2. (A). The KEGG pathway enrichment analysis of the upregulation and downregulation of DEGs. Gene ontology enrichment analysis of the upregulated and downregulated DEGs between MS from MCF-7 vs. T47D, as analyzed by ShinyGO, including (B) Biological process, (C) Cellular component, and (D) Molecular function. (E) Drug-gene association analysis of the upregulation and downregulation of DEGs, and (F). Disease-gene association analysis of the upregulated and downregulated DEGs between MS from MCF-7 vs. T47D, as analyzed by WebGestalt. KEGG: Kyoto Encyclopedia of Genes and Genomes; DEGs: differentially expressed genes.

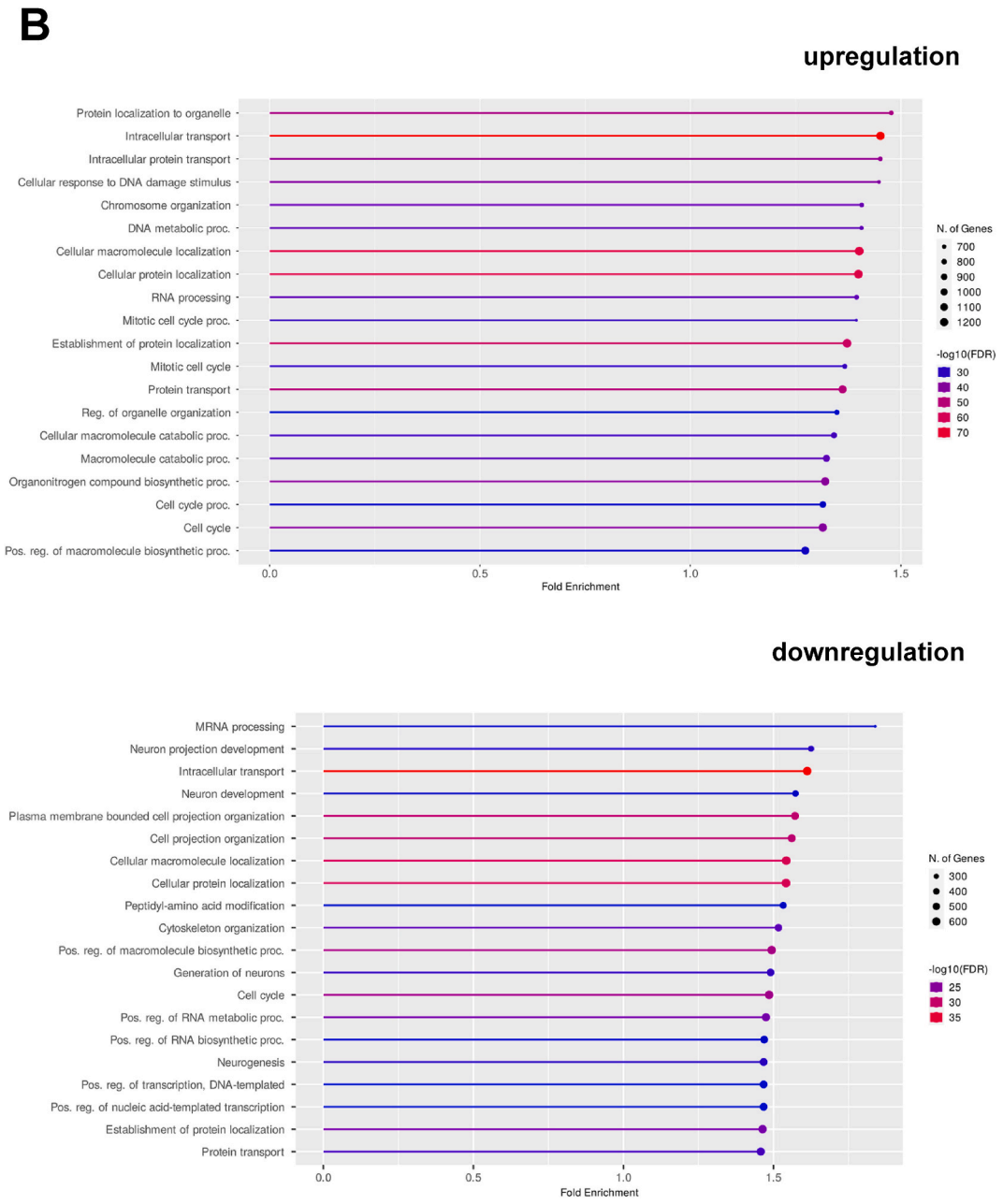

Fig. 2. (*continued*).

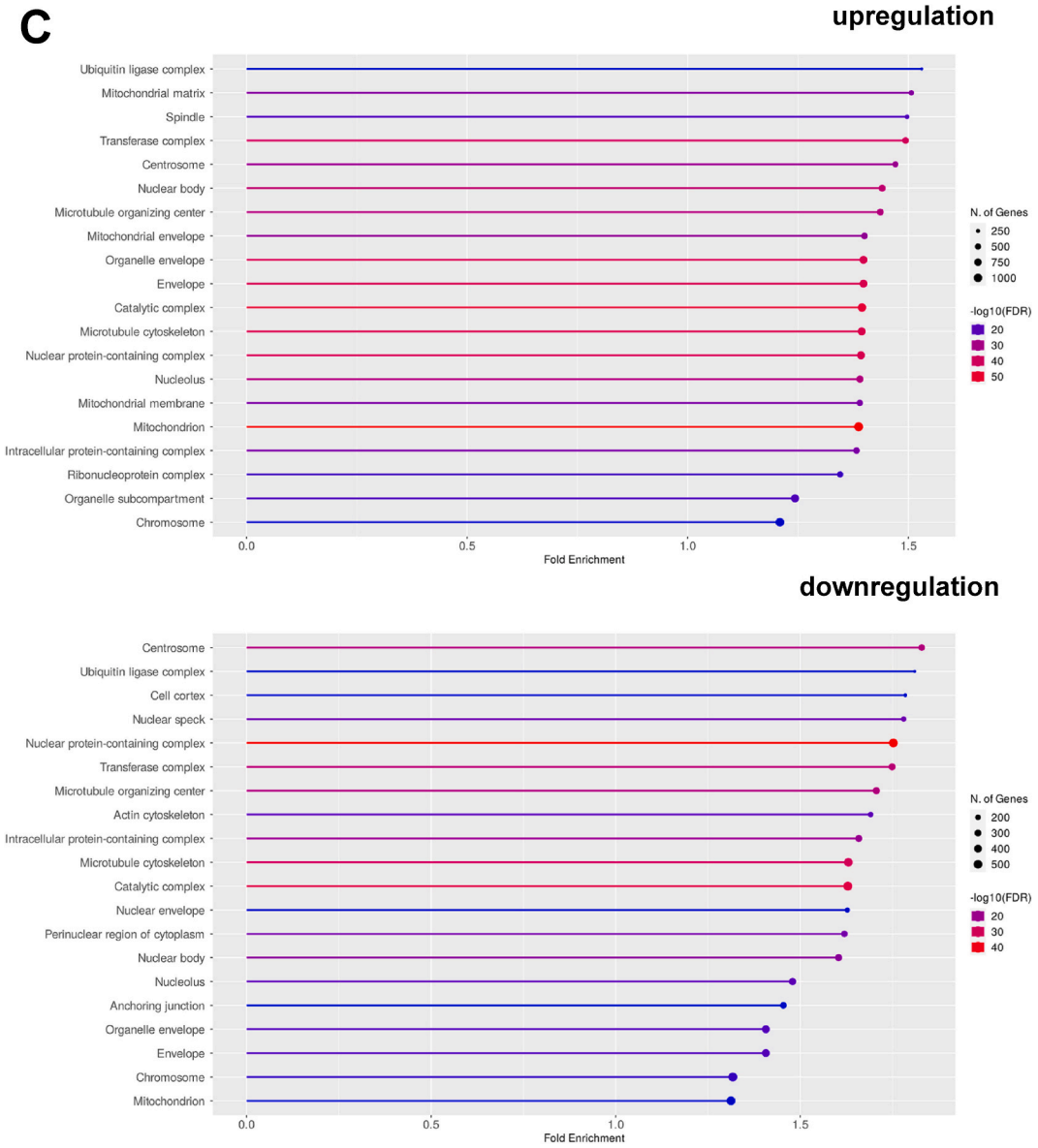

Fig. 2. (*continued*).

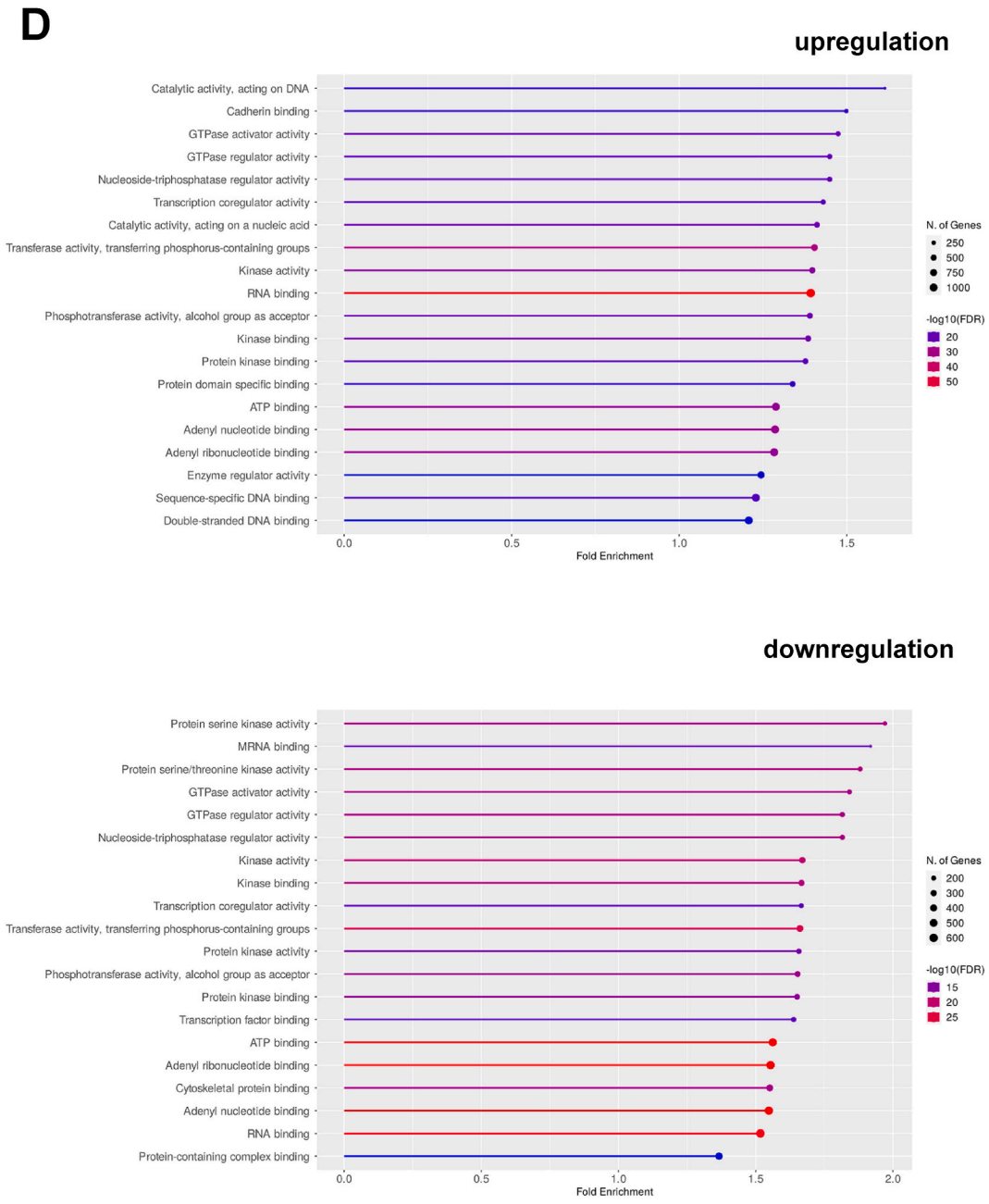

Fig. 2. (*continued*).

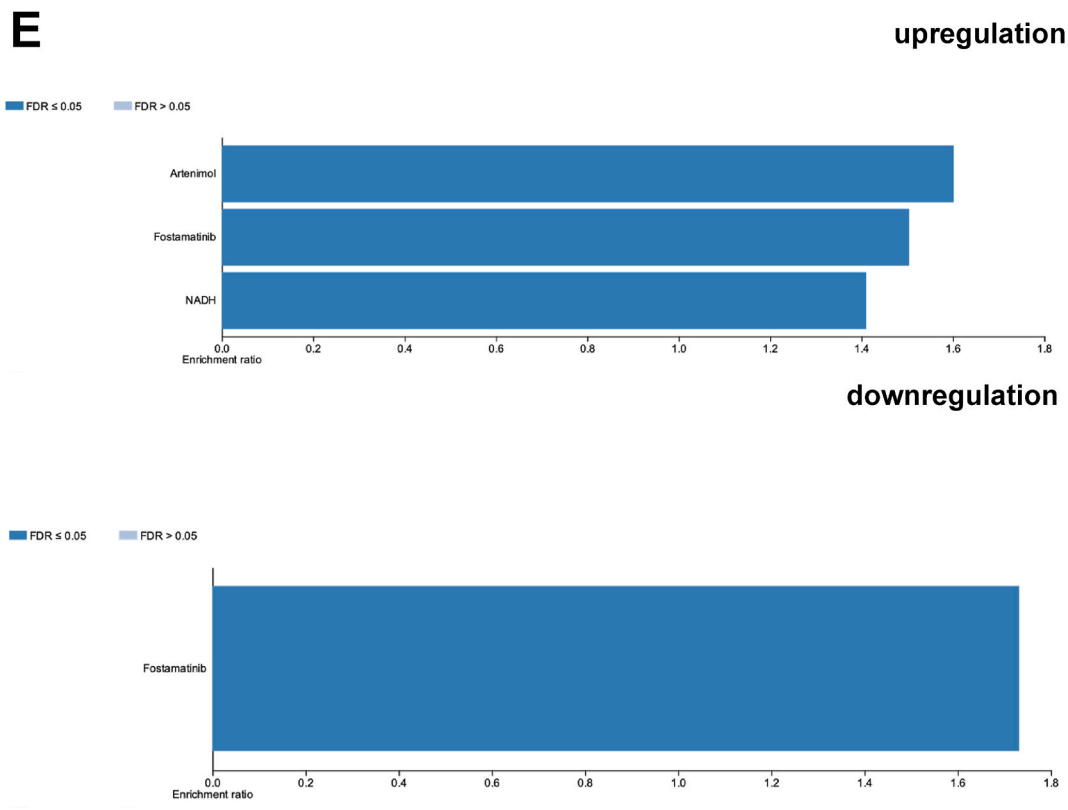

Fig. 2. (*continued*).

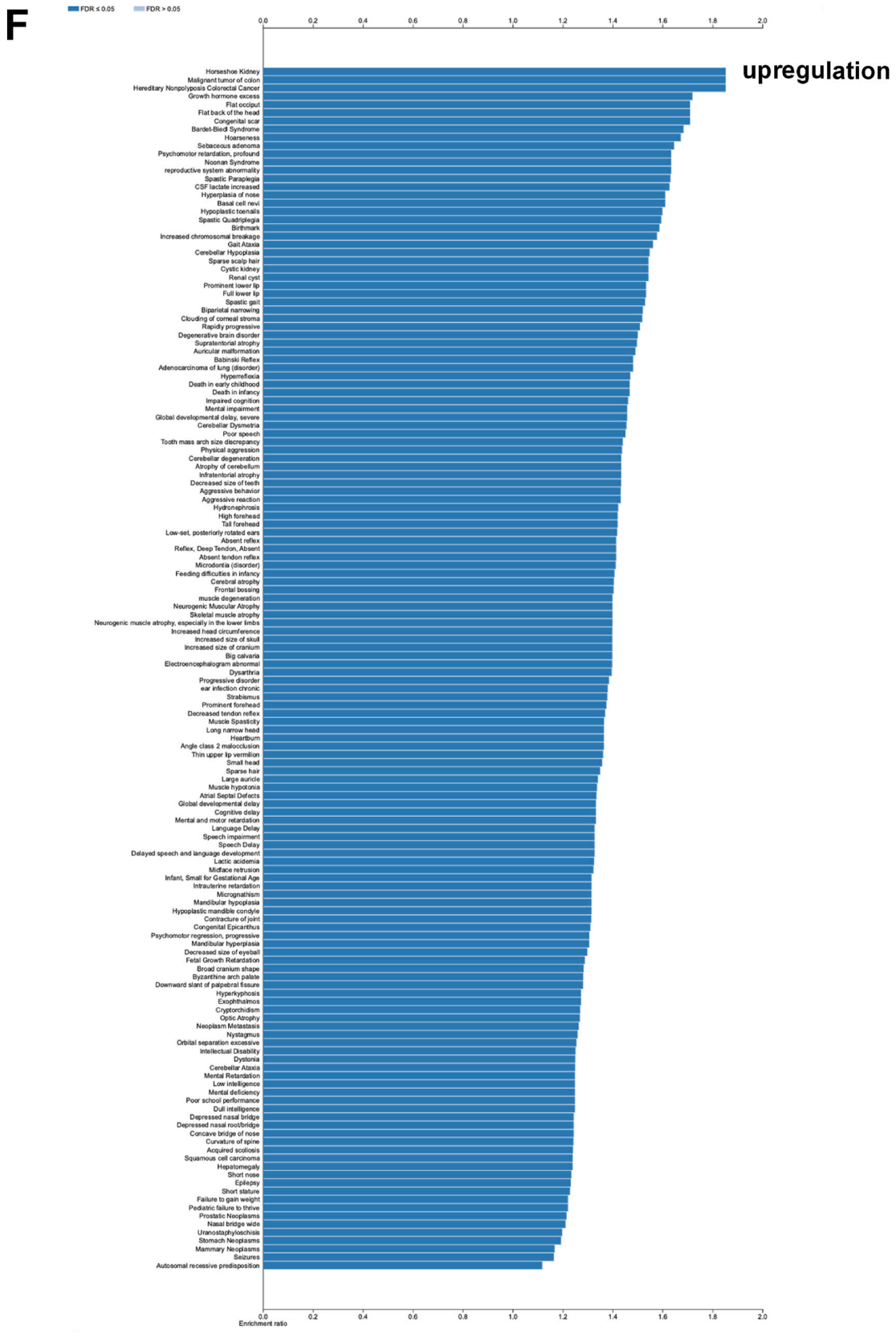

Fig. 2. (*continued*).

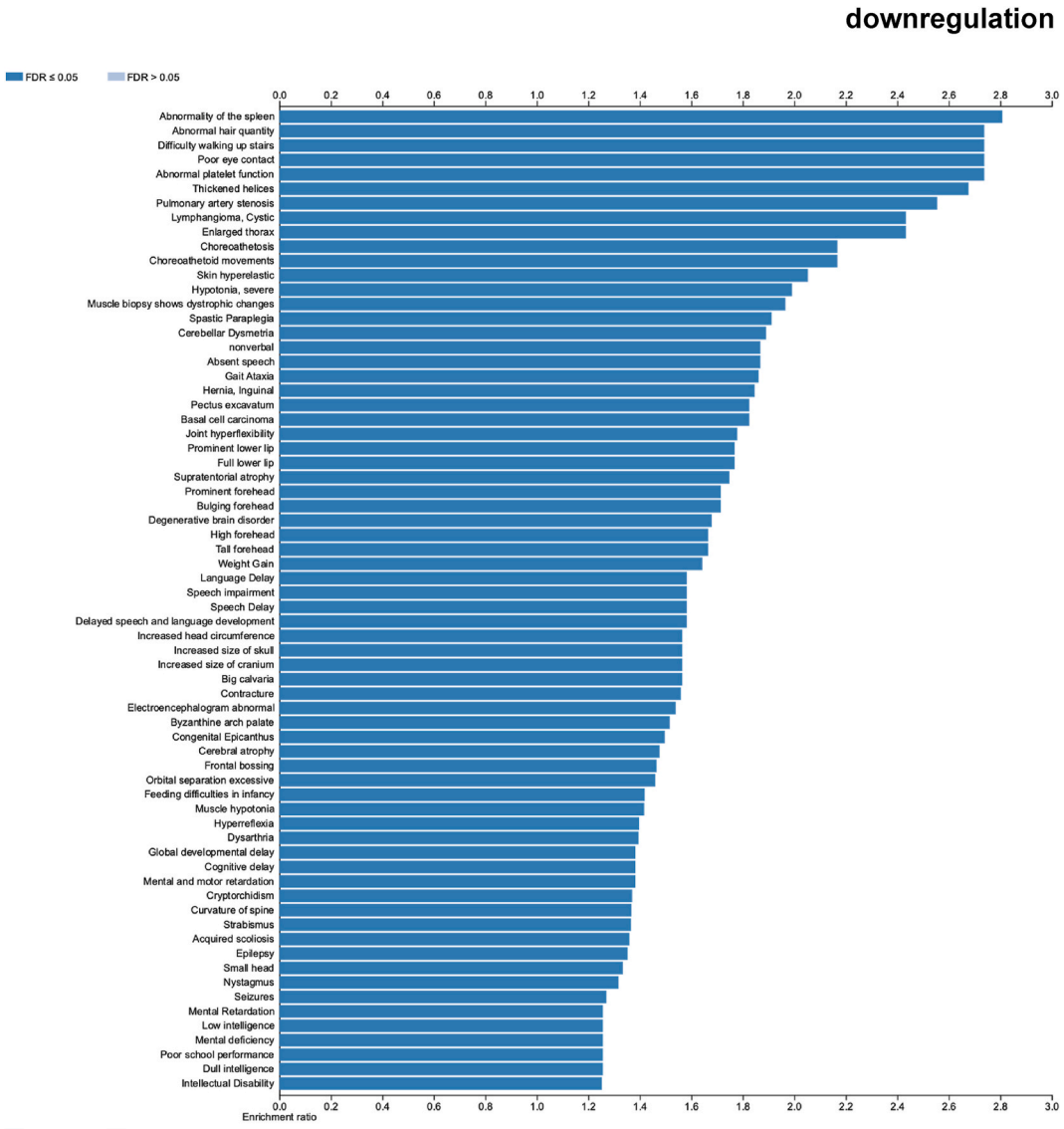

Fig. 2. (*continued*).

the expression levels of *SOX2, CD133, ALDH1, NANOG*, and *OCT4* were significantly upregulated than in MCF-7 cells. In T47D MS, the expression levels of *CD133*, *ALDH1*, and *OCT4* were significantly upregulated than in T47D cells. Subsequently, we performed next-generation sequencing on RNA isolated from the MS, revealing 40,940 DEGs, consisting of 34,047 upregulated and 6,893 downregulated genes (Supplementary Table 2). The top 10 upregulated genes were *PKM, NDRG1, LDHA, ERO1A, IGFBP3, ACTG1, RPL13A, SLC6A6, EPAS1*, and *NCOA3*, whereas the top 10 downregulated genes were *APLP2, MSN, RPL10L, GSTP1, CXCL3, NEDD4, RPL23P8, AKR1B1, SDCBP,* and *ST13* (Table 1).

3.2. KEGG pathway and GO enrichment analyses

We performed KEGG pathway enrichment analysis on the upregulated and downregulated DEGs. The upregulated DEGs were enriched in several KEGG pathways, including ubiquitin-mediated proteolysis, lysosome, endocytosis, and metabolic pathways (Fig. 2A, top panel). The downregulated DEGs were enriched in pathways related to adherens junctions, cellular senescence, MAPK signaling, and metabolic processes (Fig. 2A, bottom panel). GO enrichment analysis was performed in three phases: biological process, cellular component, and molecular function. The upregulated DEGs were associated with regulating biological processes such as intracellular transport, DNA metabolic processes, mitotic cell cycle, cellular macromolecule catabolic processes, and organonitrogen compound biosynthesis (Fig. 2B, top panel). The downregulated DEGs were associated with processes such as intracellular transport, cell cycle, establishment of protein localization, and protein transport (Fig. 2B, bottom panel).

The upregulated DEGs were located in the ubiquitin–ligase complex, mitochondrial matrix, spindle, catalytic complex, and intracellular protein-containing complex (Fig. 2C, top panel), whereas the downregulated DEGs were located in the centrosome, ubiquitin ligase complex, transferase complex, chromosome, and mitochondria (Fig. 2C, bottom panel). Furthermore, the upregulated DEGs played a pivotal role in the molecular function of catalytic activities acting on DNA, GTPase activator activity, protein kinase binding, and RNA binding (Fig. 2D, top panel), whereas the downregulated DEGs were enriched for molecular functions such as protein serine kinase activity, ATP binding, protein kinase binding, and GTPase regulator activity (Fig. 2D, bottom panel).

3.3. Drug-gene and disease-gene association analysis

Drug-gene association analysis of the upregulated and downregulated DEGs revealed that both DEGs were enriched for fostamatinib (Fig. 2E). Disease-gene association analysis indicated an association between upregulated DEGs and mammary neoplasms, whereas the downregulated DEGs were enriched in basal cell carcinoma (Fig. 2F).

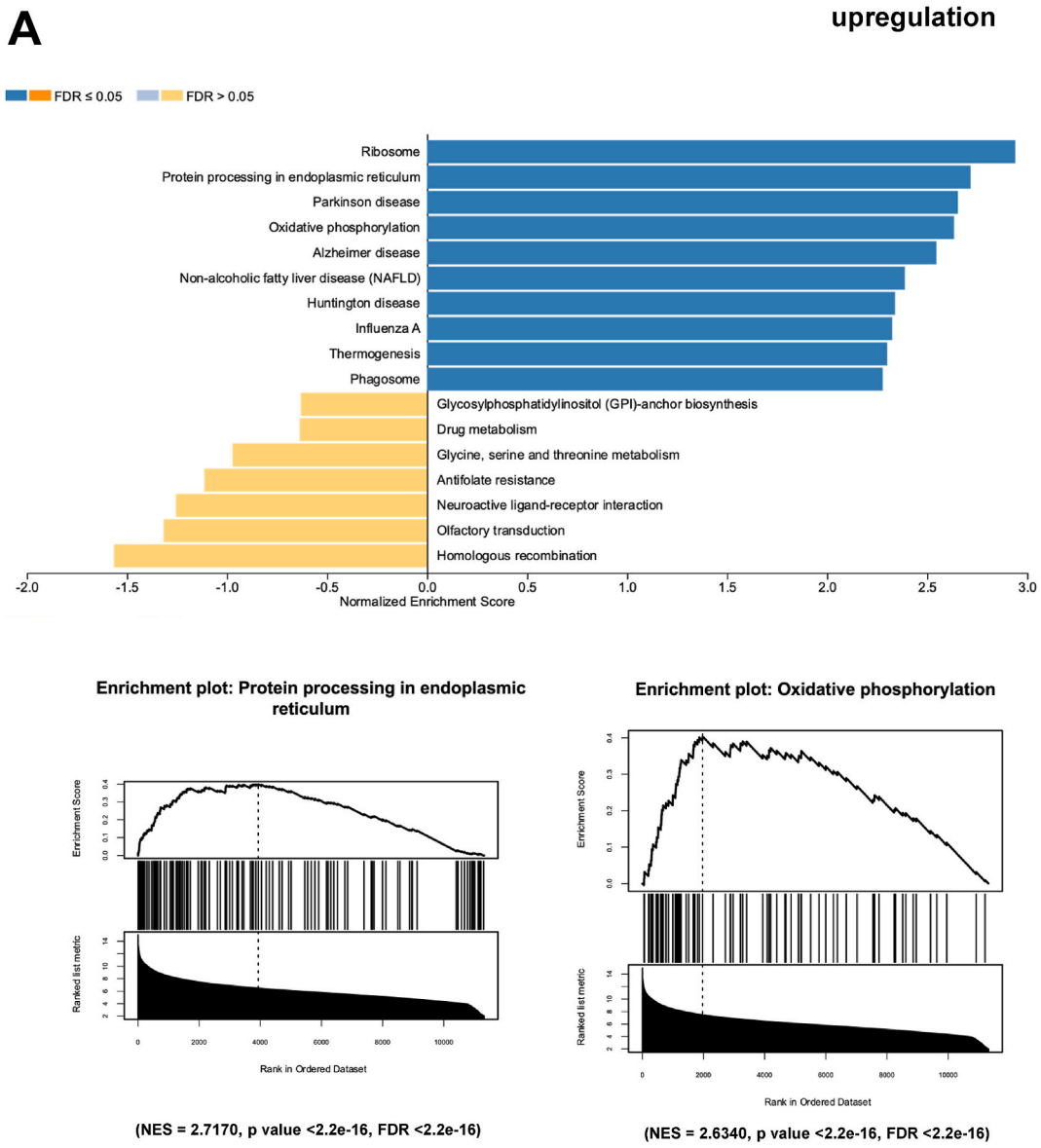

Fig. 3. (A) Bar graph and the enrichment plot of the GSEA results of upregulated DEGs show that they were positively enriched with protein processing in the endoplasmic reticulum (NES = 2.7170, $p < 2.2e\text{-}16$, FDR <2.2e-16) and oxidative phosphorylation (NES = 2.6340, $p < 2.2e\text{-}16$, FDR <2.2e-16). (B). Bar graph and the enrichment plot of the GSEA results of the downregulated DEGs show that they were negatively enriched p53-signaling pathway (NES = −1.9405, $p = 0.0010460$, FDR = 0.032027) and platinum drug resistance (NES = −2.0426, $p < 2.2e\text{-}16$, FDR = 0.013217). GSEA, Gene Set Enrichment Analysis; NES, normalized enrichment score; FDR, false discovery rate; DEGs, differentially expressed genes.

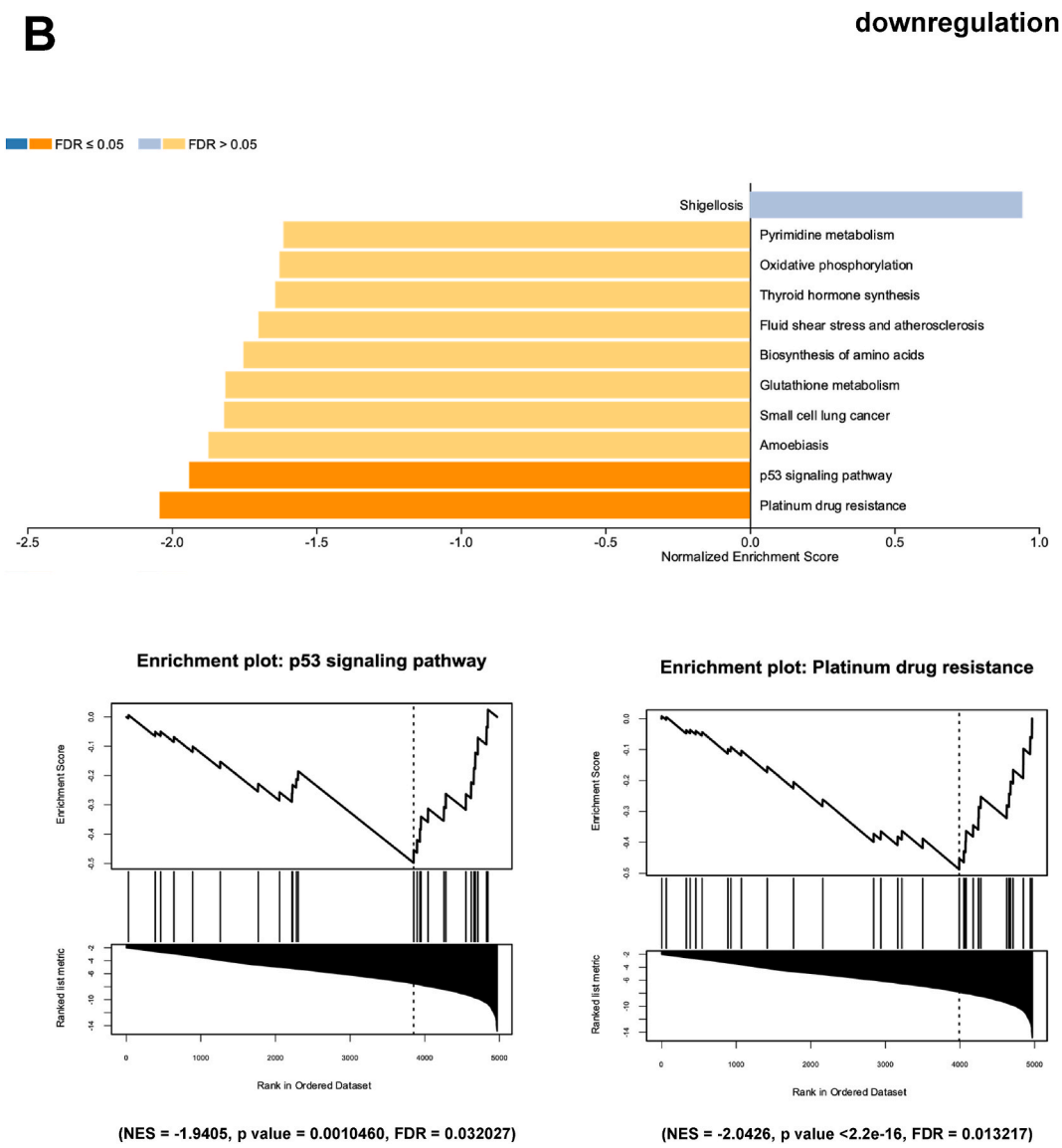

Fig. 3. (*continued*).

3.4. GSEA

Considering the limited number of samples for NGS, we focused on comprehensive DEGs profiling based on log fold change as a rank gene expression selection method. GSEA was performed to determine the biological significance of BCSC feature maintenance in MCF-7 and T47D spheroids. GSEA results from the upregulated DEGs, based on the KEGG pathway database, revealed significant enrichment in several pathways (Fig. 3A, Supplementary Table 3), including protein processing in the endoplasmic reticulum (NES = 2.7170, $p <$ 2.2e-16, FDR <2.2e-16) and oxidative phosphorylation (NES = 2.6340, $p <$ 2.2e-16, FDR <2.2e-16). The GSEA results of downregulated DEGs were negatively enriched in several signaling pathways (Fig. 3B–Supplementary Table 4), such as the p53 signaling pathway (NES = −1.9405, p = 0.0010460, FDR = 0.032027) and platinum drug resistance (NES = −2.0426, $p <$ 2.2e-16, FDR = 0.013217).

3.5. DNA methylation analysis

A heatmap was generated to depict the DNA methylation patterns and assess the predictive significance of clustering the expression levels of the top 10 upregulated and top 10 downregulated DEGs in breast cancer (Supplementary Fig. 1). The analysis of DNA methylation expression levels revealed that specific CpG sites exhibited significantly elevated levels of methylation as demonstrated by a notable prognostic significance in context of breast cancer ($p < 0.05$, determined by the likelihood ratio test). These CpG sites

Table 2
The prognostic significance of a single CpG site within the *PKM2, ERO1L, IGFBP3, SLC6A6, EPAS1, NCOA3, APLP2, RPL10L, and NEDD4* genes in breast cancer is evaluated using the MethSurv platform. The criterion for determining statistical significance was a p-value of less than 0.05 as determined by the likelihood ratio test. A notable differential expression pattern was seen in the *PKM2, ERO1L, SLC6A6, EPAS1, APLP2, RPL10L*, and *NEDD4* genes between low- and high-risk cohorts in relation to breast cancer. * : $p < 0.05$.

Name	HR	CI	Wald_P-value
PKM2 − 5′UTR−Open_Sea−cg07565018	0.527	(0.317; 0.877)	0.014*
ERO1L − TSS1500−S_Shore−cg08136587	0.542	(0.367; 0.801)	0.0021*
ERO1L − TSS1500−S_Shore−cg08554114	0.68	(0.462; 1.002)	0.051
IGFBP3 − 3′UTR−Open_Sea−cg00419512	1.433	(0.968; 2.121)	0.072
IGFBP3 − 3′UTR−Open_Sea−cg05867388	1.474	(0.988; 2.201)	0.057
IGFBP3 − 3′UTR−Open_Sea−cg06789764	0.795	(0.539; 1.171)	0.25
SLC6A6 − Body−Open_Sea−cg03371447	0.508	(0.302; 0.856)	0.011*
SLC6A6 − Body−Open_Sea−cg07056242	1.312	(0.744; 2.314)	0.35
EPAS1 − Body−Open_Sea−cg00097800	0.469	(0.275; 0.8)	0.0055*
EPAS1 − Body−Open_Sea−cg10507988	0.662	(0.402; 1.091)	0.11
EPAS1 − Body−Open_Sea−cg05943554	1.221	(0.778; 1.917)	0.38
NCOA3 − Body−Open_Sea−cg14411425	0.565	(0.34; 0.941)	0.028*
APLP2 − Body; 3′UTR−Open_Sea−cg18244874	0.669	(0.441; 1.013)	0.057
APLP2 − Body; 3′UTR−Open_Sea−cg21498950	0.577	(0.351; 0.95)	0.031*
APLP2 − Body; 3′UTR−Open_Sea−cg04626721	0.727	(0.445; 1.187)	0.2
APLP2 − Body−Island−cg24753148	0.603	(0.386; 0.941)	0.026*
RPL10L − 5′UTR; 1stExon−Island−cg02259232	0.745	(0.464; 1.194)	0.22
RPL10L − 1stExon−Island−cg25610245	1.38	(0.829; 2.297)	0.22
RPL10L − TSS200−Island−cg05282641	1.077	(0.664; 1.747)	0.76
RPL10L − TSS200−Island−cg14871534	0.546	(0.328; 0.909)	0.02*
RPL10L − TSS200−Island−cg23370328	0.748	(0.507; 1.104)	0.14
NEDD4 − Body−Open_Sea−cg16068383	0.583	(0.393; 0.865)	0.0073*
NEDD4 − Body−N_Shore−cg20929476	0.395	(0.266; 0.586)	3.80E-06*

included cg07565018 from *PKM2* ($p = 0.014$), cg08136587 from *EROL1* ($p = 0.0021$), cg03371447 from *SLC6A6* ($p = 0.011$), cg00097800 from *EPAS1* ($p = 0.0055$), cg14411425 from *NCOA3* ($p = 0.028$), cg21498950 ($p = 0.031$) and cg24753148 ($p = 0.026$) from *APLP2*, cg14871534 ($p = 0.02$) from *RPL10L*, and cg16068383 ($p = 0.0073$) and cg20929476 ($p = 3.80E-06$) from *NEDD4* (Table 2).

3.6. Correlation analysis of immune cell infiltration with DEGs

The TIMER database was used to investigate the immunological milieu and identify associations between immune infiltration levels and the top 10 upregulated and downregulated DEGs in breast cancer (Table 3, Supplementary Fig. 2). The expression of *SLC6A6* exhibited a moderate and statistically significant positive correlation with macrophage infiltration ($r = 0.425$, $p = 9.37E-45$). There was a significant negative association between the expression of *EPAS1* and purity ($r = -0.401$, $p = 8.71E-40$), with a moderate effect size. *MSN* expression levels exhibited a significant positive correlation with neutrophil ($r = 0.691$, $p = 5.59E-142$) and dendritic cell ($r = 0.462$, $p = 1.08E-53$) infiltration. Furthermore, *AKR1B1* expression showed a significant negative correlation with purity ($r = -0.434$, $p = 4.88E-47$) and significant positive correlations with neutrophil ($r = 0.499$, $p = 1.32E-63$) and dendritic cell ($r = 0.48$, $p = 1.63E-58$) infiltration.

The expression of *SLC6A6* exhibited a moderate and statistically significant positive correlation with macrophage infiltration ($r = 0.425$, $p = 9.37E-45$). There was a significant negative association between the expression of *EPAS1* and purity ($r = -0.401$, $p = 8.71E-40$), with a moderate effect size. *MSN* expression levels exhibited a significant positive correlation with neutrophil ($r = 0.691$, $p = 5.59E-142$) and dendritic cell ($r = 0.462$, $p = 1.08E-53$) infiltration. Furthermore, *AKR1B1* expression showed a significant negative correlation with purity ($r = -0.434$, $p = 4.88E-47$) and significant positive correlations with neutrophil ($r = 0.499$, $p = 1.32E-63$) and dendritic cell ($r = 0.48$, $p = 1.63E-58$) infiltration.

3.7. Association analysis between genes and small molecule compounds using CMap

Using the CMap database, we identified 15 drugs/molecules that exhibited positive correlations, and 15 drugs/molecules that displayed negative correlations (Table 4). SA-83851 was identified as a potential compound with the ability to reverse gene expression patterns associated with mutant TP53. Conversely, compounds, including BRD-K14027855, indirubin, mefloquine, SR-33805, clonazepam, GW-5074, BRD-K61033289, fingolimod, ciclopirox, SPB02137, PTMS, kenpaullone, capsazepine, exemestane, and BRD-K00540336, were projected to reverse-generate gene expression similar to the DEGs between MS derived from MCF-7 and T47D cells.

4. Discussion

In this study, we explored the differences in the mammosphere transcriptomic profiles of MCF-7 and T47D breast cancer cells. The upregulated DEGs implied that the genes were upregulated in MS derived from MCF-7 cells, whereas the downregulated DEGs or genes

Table 3
Immune cell infiltration related to the expression levels of *PKM2, NDRG1, LDHA, EROA1, IGFBP3, ACTG1, RPL13A, SLC6A6, EPAS1, NCOA3, APLP2, MSN, RPL10L, GSTP1, CXCL3, NEDD4, RPL23P8, AKR1B1, SDCBP,* and *ST13*. The value of Spearman's Rank Correlation Coefficient (positive or negative) was consider a very weak correlation (0.00–0.19), a weak correlation (0.20–0.39), a moderate correlation (0.40–0.69), a strong correlation (0.70–0.89), and a very strong correlation (0.90–1.0). Bold indicates significant value ($p < 0.05$) and a moderate correlation.

Gene Name	Parameters	Purity	B cell	$CD8^+$	$CD4^+$	Macrophage	Neutrophil	Dendritic cell
PKM2	R	0.025	−0.031	0.079	−0.088	0.109	0.111	0.137
	P value	4.22E-01	3.34E-01	1.29E-02	5.62E-03	5.92E-04	4.41E-04	1.46E-05
NDRG1	R	0.005	−0.196	−0.054	0.004	−0.02	0.271	0.194
	P value	8.77E-01	4.42E-10	8.86E-02	8.89E-01	5.22E-01	3.15E-18	7.39E-10
LDHA	R	0.085	−0.059	0.133	−0.252	0.228	0.288	−0.021
	P value	7.05E-03	6.26E-02	2.77E-05	7.25E-16	3.60E-13	1.99E-20	5.12E-01
EROA1	R	−0.014	−0.198	0.256	−0.312	0.301	0.373	0.101
	P value	6.62E-01	3.00E-10	2.22E-16	7.54E-03	3.03E-22	4.40E-34	1.37E-03
IGFBP3	R	−0.3	−0.199	0.192	−0.05	0.202	0.346	0.252
	P value	3.77E-22	2.42E-10	1.06E-09	1.15E-01	1.25E-10	2.09E-29	8.08E-16
ACTG1	R	0.047	−0.092	0.084	−0.077	0.141	0.095	0.04
	P value	1.34E-01	3.54E-03	8.25E-03	1.55E-02	8.62E-06	2.62E-03	2.09–01
RPL13A	R	−0.136	0.001	−0.119	0.181	−0.163	−0.263	−0.02
	P value	1.69E-05	9.83E-01	1.66E-04	9.25E-09	2.28E-07	3.69E-17	9.39E-01
SLC6A6	R	−0.185	−0.069	0.231	−0.04	**0.425**	0.335	0.133
	P value	3.94E-09	2.91E-02	1.77E-13	2.05E-01	**9.37E-45**	1.95E-27	2.68E-05
EPAS1	R	**−0.401**	−0.17	0.281	0.006	0.277	0.187	0.208
	P value	**8.71E-40**	6.55E-08	1.63E-19	8.53E-01	5.03E-19	3.02E-09	3.65E-11
NCOA3	R	0.018	0.023	0.31	−0.106	0.351	0.285	−0.007
	P value	5.73E-01	4.73E-01	1.45E-23	7.97E-04	3.06E-30	5.48E-20	8.31E-01
APLP2	R	0.023	−0.127	0.114	−0.184	0.237	−0.047	−0.106
	P value	4.65E-01	6.29E-05	3.26E-04	5.04E-09	4.13E-14	1.39E-01	8.32E-04
MSN	R	−0.388	−0.228	0.207	0.13	0.273	**0.691**	**0.462**
	P value	4.08E-37	3.09E-13	4.15E-11	4.02E-05	2.09E-18	**5.59E-142**	**1.08E-53**
RPL10L	R	−0.012	−0.01	−0.029	0	−0.026	−0.005	−0.039
	P value	7.09E-01	7.49E-01	3.64E-01	9.94E-01	4.10E-01	8.66E-01	2.25E-01
GSTP1	R	−0.073	−0.098	−0.278	0.184	−0.155	0.269	0.343
	P value	3.40E-01	2.02E-03	2.09E-04	5.06E-09	9.57E-07	5.98E-18	7.62E-29
CXCL3	R	−0.336	−0.231	−0.106	0.17	−0.111	0.39	0.307
	P value	1.01E-27	1.84E-13	7.95E-04	6.48E-08	4.46E-04	1.67E-37	3.75E-23
NEDD4	R	−0.104	−0.092	0.399	−0.219	0.492	0.167	−0.03
	P value	1.08E-03	3.54E-03	2.71E-39	2.76E-12	1.13E-61	1.20E-07	3.45E-01
RPL23P8	R	−0.043	−0.067	0.017	0.008	−0.092	−0.143	−0.05
	P value	1.79E-01	3.57E-02	5.95E-01	7.90E-01	3.60E-03	5.46E-06	8.17E-02
AKR1B1	R	**−0.434**	−0.081	0.058	0.125	0.24	**0.499**	**0.48**
	P value	**4.88E-47**	1.05E-02	6.91E-02	8.25E-05	1.54E-14	**1.32E-63**	**1.63E-58**
SDCBP	R	−0.215	−0.204	0.209	−0.046	0.337	**0.491**	0.229
	P value	6.64E-12	8.54E-11	2.78E-11	1.48E-01	9.01E-28	**1.95E-61**	2.89E-13
ST13	R	0.018	−0.089	0.174	−0.229	0.275	0.085	−0.141
	P value	2.01E-04	4.49E-03	3.53E-08	2.77E-13	1.10E-18	7.00E-03	7.95E-06

were downregulated in MCF-7 MS or upregulated in T47D cells. The top 10 upregulated genes were *PKM, NDRG1, LDHA, ERO1A, IGFBP3, ACTG1, RPL13A, SLC6A6, EPAS1*, and *NCOA3*, whereas the top 10 downregulated genes were *APLP2, MSN, RPL10L, GSTP1, CXCL3, NEDD4, RPL23P8, AKR1B1, SDCBP,* and *ST13*.

PKM2 encodes pyruvate kinase M2, a critical rate-limiting enzyme in glycolysis responsible for converting phosphoenolpyruvate to pyruvate [24]. PKM2-mediated glycolysis plays a crucial role in enabling triple-negative breast cancer cells to maintain the $CD44+CD24^-$phenotype and exhibit BCSC characteristics, such as mammosphere formation and *in vivo* initiation of tumor growth [25]. *NDRG1* encodes N-myc downstream regulated gene 1 (NDRG1), which is known to be responsive to the presence of nickel and calcium and is involved in various crucial processes related to the initial development of cancerous tumors, as well as their invasion and spread to other parts of the body [26]. The overexpression of *NDRG1*facilitates the acquisition of stem-like characteristics in non-small cell lung cancer, including enhanced sphere-forming capacity and tumorigenic potential [27]. *LDHA* encodes lactate dehydrogenase A (LDHA), a key enzyme in glycolysis responsible for converting pyruvate to lactate. Elevated LDHA levels have been observed in various malignancies, contributing to cancer progression [28]. BCSCs exhibit elevated levels of glycolytic proteins, namely PKM2 and LDHA, along with increased pyruvate kinase and lactate dehydrogenase activities [29].

Furthermore, *ERO1A* encodes endoplasmic reticulum oxidoreductin-1 alpha (ERO1α), which is located in the endoplasmic reticulum (ER) and undergoes oxidative cycles in collaboration with protein disulfide isomerase (PDI). This process facilitates protein folding and contributes to maintaining ER homeostasis [30]. The overexpression of ERO1α facilitates the advancement of tumors under hypoxic conditions, specifically in pancreatic cancer, and is linked to a poor prognosis in patients with this type of cancer [31]. *IGFBP3* encodes insulin-like growth factor-binding protein 3 (IGFBP-3) and is induced by hypoxia. IGFBP-3 plays a regulatory role in several biological processes, including cell proliferation, senescence, apoptosis, and epithelial-mesenchymal transition [32]. Moreover, IGFBP3 promotes tumor growth by inducing a fraction of tumor cells with high CD44 expression, a key hyaluronic acid cell

Table 4
Identification of several promising therapeutic for DEGs of BCSCs from MCF-7 vs. T47D mammospheres through the utilization of CMap analysis.

Rank	CMapName	Cells	Dosage	Time	Mechanism of Action	Connectivity Score
1	BRD-K14027855	MCF7	10 μM	6 h		0.43
2	indirubin	MCF7	10 μM	24 h	CDK inhibitor	0.43
3	mefloquine	MCF7	10 μM	6 h	Adenosine receptor antagonist	0.43
4	SR-33805	MCF7	10 μM	24 h	Calcium channel blocker	0.42
5	clonazepam	MCF7	10 μM	24 h	GABA receptor agonist	0.42
6	GW-5074	MCF7	10 μM	24 h	–	0.42
7	BRD-K61033289	MCF7	10 μM	48 h	PPAR receptor agonist	0.42
8	fingolimod	MCF7	10 μM	24 h	Sphingosine 1 phosphate receptor agonist	0.41
9	ciclopirox	MCF7	10 μM	6 h	Membrane integrity inhibitor	0.4
10	SPB02137	MCF7	10 μM	6 h	–	0.4
11	PTMS	MCF7	–	96 h	–	0.4
12	kenpaullone	MCF7	10 μM	24 h	CDK inhibitor/GSK inhibitor	0.39
13	capsazepine	MCF7	10 μM	6 h	TRPV agonist	0.39
14	exemestane	MCF7	10 μM	48 h	Aromatase inhibitor	0.39
15	BRD-K00540336	MCF7	20 μM	24 h	–	0.39
38759	YWHAQ	MCF7	–	96 h	–	−0.39
38760	SA-83851	MCF7	0.37 μM	6 h	–	−0.39
38761	KCNK1	MCF7	2 μL	144 h	–	−0.39
38762	SMARCC2	MCF7	–	96 h	–	−0.39
38763	SORT1	MCF7	–	96 h	–	−0.4
38764	GABRB3	MCF7	–	96 h	–	−0.4
38765	SPR	MCF7	–	96 h	–	−0.4
38766	EIF4G1	MCF7	–	144 h	–	−0.4
38767	FAS	MCF7	–	144 h	–	−0.4
38768	RAD23B	MCF7	–	144 h	–	−0.41
38769	YWHAQ	MCF7	2 μL	96 h	–	−0.41
38770	FRAT1	MCF7	–	96 h	–	−0.42
38771	NFE2L2	MCF7	–	144 h	–	−0.42
38772	ZNF385B	MCF7	–	96 h	–	−0.43
38773	PLAU	MCF7	–	144 h	–	−0.43

surface receptor implicated in invasion, metastasis, and treatment resistance [32].

Moreover, *ACTG1* encodes γ-actin, a component of the cytoskeleton involved in maintaining centrosome integrity and controlling mitosis [33]. The expression of ACTG1 is reduced in human breast cancer cells, leading to resistance to antimitotic drugs and subsequent chemoresistance [34]. *RPL13A* encodes ribosomal protein L13a (RPL13a), a member of the L13 ribosomal protein family that serves as a structural component of the large 60S ribosomal subunit and is one of the preferred ribosomal proteins for studying mesenchymal stem cells (MSCs) [35]. A previous study demonstrated that the cancer stem cell population of prostate cancer cells exhibited significantly elevated expression of RPL13a [36]. Expression of the taurine transporter SLC6A6 is significantly higher in colorectal cancer cells than in normal adjacent cells [37]. The inhibition of SLC6A6 resulted in a reduction in the population of side population (SP) cells and their cancer stem cell (CSC) characteristics, including their ability to initiate tumor formation [38].

EPAS1 encodes the endothelial PAS domain protein 1, also known as hypoxia-inducible factor 2A (HIF2A), which is a transcription factor that regulates genes associated with angiogenesis [39]. HIF2A induces the expression of OCT4, a BCSC marker [40]. Activation of the Wnt and Notch pathways by HIF-2α facilitates the transition to a stem cell phenotype and confers chemoresistance in breast cancer cells [41]. *NCOA3* encodes nuclear receptor coactivator 3, also known as amplified in breast 1 (AIB1), a constituent of the nuclear receptor co-activator family that is overexpressed in breast cancer and facilitates estrogen-induced cancer cell proliferation [42]. Moreover, AIB1 can potentially enhance resistance to anti-hormone therapy and promote BCSC activity by improving metabolic adaptability through its interaction with PELP1 [43].

Furthermore, *APLP2* encodes amyloid precursor-like protein 2 (APLP2), and its overexpression has been observed in cancer cells and associated with increased levels of tumor cell proliferation, migration, and invasion [44]. APLP2 functions as a tumor promoter in hepatocellular carcinoma by impeding programmed cell death (apoptosis) and promoting cell growth [45]. *MSN* encodes moesin, a member of the ezrin and radixin (ERM) family. Moesin connects the actin cytoskeleton to transmembrane receptors [46] and plays a role in the metastasis of pancreatic cancer cells [47]. It also serves as an independent prognostic marker for ER-positive breast cancer [48]. The differential regulation of Src activity and β-catenin translocation to the nucleus in breast cancer cells is influenced by intracellular and external moesin [49]. *RPL10L* encodes the ribosomal protein L10 like (RPL10L), a component of the ribosome, and the overexpression of RPL10 results in enhanced cell viability, motility, and invasion, while concurrently reducing cellular death in epithelial ovarian cancer cells [50]. A previous study demonstrated that RPL10 UFMylation plays a significant role in augmenting the stemness of pancreatic cancer cells, thereby contributing to the formation of pancreatic adenocarcinoma [51].

Moreover, *GSTP1* encodes glutathione S-transferase P-1 (GSTP1), a member of a cluster of isoenzymes that participate in the second phase of xenobiotic detoxification through glutathione conjugation [52]. GSTP1 is a cancer stem cell marker of hepatocellular carcinoma [53]. Cisplatin resistance in lung CSCs can be attributed to the transcriptional activation of Gstp1 expression, which is mediated by the MEK/ERK signaling pathway [54]. GSTP1 is a therapeutic target for inhibiting lung adenocarcinoma stemness and overcoming resistance to tyrosine kinase inhibitors [55]. *CXCL3* encodes C-X-C motif chemokine ligand 3 (CXCL3), a member of the

CXC chemokine family. CXCL3 attracts neutrophils and promotes cancer initiation, angiogenesis, and metastasis [56]. The suppression of CXCL3 results in the inhibition of the JAK2/STAT3 signaling pathway, which is essential for the proliferation of $CD44^{+}/CD24^{-}$ stem cell-like cells in human breast cancer [57]. Furthermore, *NEDD4* encodes neural precursor cells expressing developmentally downregulated protein 4 (NEDD4), an E3 ubiquitin ligase that regulates the stability and subcellular distribution of target proteins via proteasomal degradation [58]. NEDD4 expression has been associated with the advancement of breast cancer and can serve as a predictive factor for poor prognosis [59]. NEDD4 plays a significant role in regulating the populations and phenotypic traits of BCSCs [60].

RPL23P8 encodes ribosomal protein L23 pseudogene 8 (RPL23P8). RPL23P8 variants have been associated with prostate cancer in Europeans in a genome-wide association study [61]. Furthermore, *AKR1B1* encodes aldo-keto reductase family 1, member B1 (AKR1B1), which plays a significant role in the regulation of glucose metabolism and osmoregulation, while providing support for the mitigation of superoxides and harmful substances [62]. The overexpression of *AKR1B1* is associated with basal-like breast cancer and serves as a prognostic indicator for unfavorable outcomes in patients with breast cancer [63]. Specifically, increased *AKR1B1* expression promotes tumorigenicity and metastasis in patients with breast cancer [63]. The expression levels of CSC markers decrease following the suppression of AKR1B1 in cell lines derived from lung and breast cancers [64]. *SDCBP* encodes syndecan-binding protein (SDCBP) or synthenin, an adapter protein with the ability to modulate intracellular transport of transmembrane proteins [65]. A previous study observed a correlation between elevated plasma SDCBP levels and poor treatment outcomes in patients with advanced non-small cell lung cancer who received platinum-based chemotherapy [66]. SDCBP increased the growth of gastric carcinoma by stimulating proliferation cell nuclear antigen expression and reducing gastric carcinoma cell death via the inhibition of the PI3K/AKT/mTOR pathway [67]. Lastly, *ST13* encodes ST13 Hsp70 interacting protein (HIP) [68]. *ST13* regulates cellular proliferation, inhibits tumor growth in colorectal cancer and may influence cell migration [69]. The downregulation of *ST13* is associated with platinum-based chemotherapy resistance in overian cancer [70].

Drug-gene association analysis showed that both upregulated and downregulated DEGs were enriched for fostamatinib. Disease-gene association analysis suggested that upregulated DEGs were enriched in mammary neoplasms, while downregulated DEGs were associated with basal cell carcinoma. Furthermore, upregulated DEGs exhibited enrichment in oxidative phosphorylation. Notably, CSCs primarily rely on oxidative phosphorylation as their primary energy source [71]. Previous studies have suggested that oxidative phosphorylation induces stemness properties in pancreatic cancer [72] and hepatocellular carcinoma stem cells [73]. Inhibition of oxidative phosphorylation hampers spheroid formation and increases the sensitivity of CSCs to mitochondria-targeted drugs [74].

The downregulated DEGs were negatively enriched in the p53 signaling pathway, implying that the DEGs were downregulated in the p53 signaling pathway. These results confirm, that in T47D cells, which possess mutant TP53, p53-independent signaling is activated. A missense mutation, L194F, has been identified in T47D cells [75], and has been associated with chromatin and its associated factor PARP [76]. As evidenced by the reduced TP53 transcriptional activation activity and reduced binding to BCL2 in cell culture, L194 causes the TP53 protein to lose its function [76]. Mutations in TP53 were found to increase the stemness properties of CSCs, as depicted by the increased expression of CSC markers [77]. L194F leads to the inhibition of apoptosis and cell cycle arrest by mortaparib, indicating the loss of p53 function in T47D cells [78].

Fostamatinib is a splenic tyrosine kinase (SYK) inhibitor approved for the treatment of patients with chronic immune thrombocytopenia (ITP) [79]. A clinical trial of fostamatinib has been conducted in patients with aggressive colorectal, head and neck, non-small cell lung, renal cell, and thyroid carcinomas, as well as pheochromocytomas. These trials indicated limited tumor activity but potential anti-angiogenic effects [80]. Another study showed that SYK activates PI3K/Akt signaling in Epstein–Barr virus-induced lymphoproliferation, and fostamatinib-induced apoptosis and cell cycle arrest via downregulation of PI3K/Akt signaling inhibits SYK [81]. SYK activation by PI3K/Akt promotes survival pathways and cellular resistance to oxidative stress-induced apoptosis [82]. Previous studies have demonstrated that SYK inhibition by fostamatinib reduces p53 levels and activity in HCT116 and HT1080 human colon cancer cells [83]. Additionally, SYK inhibition alters mitochondrial functions and suppresses oxidative metabolism in myeloid leukemia stem cells [84]. These previous studies collectively support the findings of this study, highlighting the relationship between fostamatinib, oxidative phosphorylation, and p53 signaling in BCSCs. This suggests that oxidative phosphorylation and p53 signaling are crucial for maintaining BCSC characteristics and serve as promising targets for BCSC therapy.

DNA methylation analysis revealed significant disparities in the gene expression of *PKM2, ERO1L, SLC6A6, EPAS1, APLP2, RPL10L*, and *NEDD4* when comparing low-risk and high-risk cohorts in the context of breast cancer. These findings align with previous studies on the methylation of these genes and their effects on cancer progression. The acetylation of PKM2 may facilitate its degradation and result in a glycolytic switch that can be rapidly deactivated in tumor cells through various mechanisms [85]. *PKM2* methylation, facilitated by CARM1, activates aerobic glycolysis, thereby facilitating breast cancer cell progression [86]. Hypomethylation plays a role in *SLC6A6* mRNA upregulation and gastric cancer cell progression [87]. Epigenetic alterations in *ERO1L* by microRNA-144-3p are involved in the development of oral squamous cell carcinoma [88]. DNA methylation of *EPAS1* leads to the downregulation of *EPAS1* mRNA and the progression of colorectal cancer cells [89]. The DNA methylation of *NEDD4* leads to *NEDD4* mRNA downregulation, reducing cell migration and invasion in gastric cancer cells [90]. Future studies on DNA methylation, in conjunction with BCSC maintenance, represent an intriguing avenue for further investigation.

A significant positive correlation was observed between the genes and macrophages, neutrophils, and dendritic cells. The correlation analysis of immune cell infiltration showed that the *SLC6A6* expression was significantly positively correlated with the macrophage infiltration, indicating a moderate association. Macrophages play a critical role in immune infiltration within tumors and have been linked to an unfavorable prognosis in breast cancer [91]. Furthermore, they actively contribute to the modulation of immune responses against tumor cells. A notable positive association was also observed between *MSN* and *AKR1B1* expression and the

invasion of neutrophils and dendritic cells. Neutrophil infiltration has been implicated in regulating pro-tumor features and therapeutic resistance [92]. Dendritic cell immunotherapy has exhibited significant promise in eliciting targeted immune responses against specific antigens, counteracting immunosuppression, and correlating with clinical response in breast cancer [93]. In summary, *SLC6A6*, *MSN,* and *AKR1B1* may serve as biomarkers of poor prognosis in breast cancer and BCSCs.

CMap analysis revealed that SA-83851, a chemical substance, possesses the potential to reverse DEGs, specifically in cells harboring mutant TP53; however, information on this compound is currently limited. Conversely, certain compounds, including BRD-K14027855, indirubin, mefloquine, SR-33805, clonazepam, GW-5074, BRD-K61033289, fingolimod, ciclopirox, SPB02137, PTMS, kenpaullone, capsazepine, exemestane, and BRD-K00540336, exhibit a gene expression reversal effect similar to the DEGs observed between MS from MCF-7 and T47D cells. For instance, indirubin inhibits tumor angiogenesis in prostate cancer cells [94] and mefloquine promotes breast cancer cell death by disrupting autophagy in prostate cancer cells [95]. Kenpaullone is a potential medication for the treatment of glioblastoma that targets glioma stem cells and overcomes chemoresistance to temozolomide [96]. The anti-leukemia effect of ciclopirox olamine is achieved by the downregulation of intracellular ferritin and the suppression of the beta-catenin- signaling pathway in acute lymphoblastic leukemia cell lines [97]. Fingolimod elicits apoptosis in tumor cells, thereby suppressing tumor progression [98]. The administration of exemestane resulted in a notable decrease in the incidence of invasive breast carcinomas among postmenopausal women with a moderate predisposition to breast cancer [99]. Taken together, these compounds warrant further investigation to determine their effects on BCSCs.

This study had several limitations. First, only one sample per group was used. In addition, the number of mapped reads between samples from MCF-7 and T47D cells was significantly different; therefore, DEG analysis was performed with significance set at $p < 0$. A larger number of samples per group can provide more reliable results, and DEG analysis can be conducted under stricter parameters. Therefore, further research is necessary to corroborate the conclusions of the present study, because the limited sample size may prevent the generalization of the results or increase the likelihood of false positives. Moreover, further functional analysis, particularly regarding deregulated mRNA or the ncRNA/mRNA axis, would significantly contribute to a more comprehensive understanding of BCSC biology. Nevertheless, this study offers valuable insights into the transcriptomic analysis of two luminal A breast cancer cell lines with different characteristics, specifically the *TP53* status. We underscore the importance of oxidative phosphorylation and p53 signaling as pivotal targets for BCSC maintenance. This study contributes to target identification for the development of anti-BCSC strategies in luminal A breast cancer.

5. Conclusions

The findings of this study revealed the transcriptomic profile of BCSC regulatory genes in MS from MCF-7 and T47D cells. We unveiled enriched KEGG pathways, including ubiquitin-mediated proteolysis, lysosomes, endocytosis, and metabolic pathways among upregulated DEGs, while downregulated DEGs were associated with the MAPK signaling pathway and metabolic pathways. Both upregulated and downregulated DEGs were enriched in fostamatinib. The GSEA results showed that the upregulated DEGs were enriched for oxidative phosphorylation, whereas the downregulated DEGs were negatively enriched for the p53 signaling pathway, thereby confirming the downregulation of the p53 signaling pathway in T47D cells. Prognostic significance of individual CpGs revealed distinct expression pattern in *PKM2*, *ERO1L*, *SLC6A6*, *EPAS1*, *APLP2*, *RPL10L*, and *NEDD4* genes between low- and high-risk breast cancer cohorts. Furthermore, we observed a significant positive correlation between the expression of *SLC6A6* and macrophage infiltration, suggesting a potential association between these variables. Additionally, a significant positive correlation was observed between the expression levels of *MSN* and *AKR1B1* and the infiltration of neutrophil and dendritic cells. Using CMap analysis, we identified SA-83851 as a potential counteractive agent against DEGs, particularly in cells harboring mutant *TP53*. Future investigations, such as *in vitro* and *in vivo* validations, are warranted to advance the development of anti-BCSC drug targets.

Funding statement

This study was supported by a Research Grant provided by the Ministry of Education, Culture, Research and Technology, Republic of Indonesia, through the Research Project PDUPT (contract nos. 1669/UN1/DITLIT/DIT-LIT/PT/2020 and 1619/UN1/DITLIT/DIT-LIT/PT/2021) and Penelitian Fundamental Regular 2023 (contract no. 3132/UN1/DITLIT/Dit-Lit/PT.March 01, 2023).

Data availability statement

The RNA sequencing data are available in the public Gene Expression Omnibus database (accession number: GSE218117).

CRediT authorship contribution statement

Adam Hermawan: Writing – review & editing, Writing – original draft, Investigation, Funding acquisition, Formal analysis, Data curation, Conceptualization. **Herwandhani Putri:** Supervision, Formal analysis, Data curation. **Nurul Fatimah:** Data curation. **Heri Himawan Prasetio:** Data curation.

Declaration of competing interest

The authors declare the following financial interests/personal relationships which may be considered as potential competing

interests:Adam Hermawan reports financial support, administrative support, and equipment, drugs, or supplies were provided by Ministry of Education, Culture, Research and Technology, Republic of Indonesia. .

Acknowledgements

PT. Genetika Science assisted with the next-generation sequencing. The authors thank Badan Penerbit dan Publikasi Universitas Gadjah Mada for their writing assistance, and Ms. Ririn Widarti and Ms. Dian Anita for their administrative support.

Appendix A. Supplementary data

Supplementary data to this article can be found online at https://doi.org/10.1016/j.heliyon.2024.e24356.

References

[1] P. Fernández-Nogueira, G. Fuster, Gutierrez-Uzquiza Á, P. Gascón, N. Carbó, P. Bragado, Cancer-associated fibroblasts in breast cancer treatment response and metastasis, Cancers 13 (13) (2021), https://doi.org/10.3390/cancers13133146.
[2] M.J. Lukey, A.A. Cluntun, W.P. Katt, M.J. Lin, J.E. Druso, S. Ramachandran, et al., Liver-type glutaminase GLS2 is a druggable metabolic node in luminal-subtype breast cancer, Cell Rep. 29 (1) (2019) 76–88.e7, https://doi.org/10.1016/j.celrep.2019.08.076.
[3] A.B. Hanker, D.R. Sudhan, C.L. Arteaga, Overcoming endocrine resistance in breast cancer, Cancer Cell 37 (4) (2020) 496–513, https://doi.org/10.1016/j.ccell.2020.03.009.
[4] T. Saha, K.E. Lukong, Breast cancer stem-like cells in drug resistance: a review of mechanisms and novel therapeutic strategies to overcome drug resistance, Front. Oncol. 12 (2022), https://doi.org/10.3389/fonc.2022.856974.
[5] D. Ghatak, D. Das Ghosh, S. Roychoudhury, Cancer stemness: p53 at the wheel, Front. Oncol. 10 (2021), https://doi.org/10.3389/fonc.2020.604124.
[6] A. Hermawan, M. Ikawati, R.I. Jenie, A. Khumaira, H. Putri, I.P. Nurhayati, et al., Identification of potential therapeutic target of naringenin in breast cancer stem cells inhibition by bioinformatics and in vitro studies, Saudi Pharmaceut. J. 29 (1) (2021) 12–26, https://doi.org/10.1016/j.jsps.2020.12.002.
[7] A. Hermawan, M. Ikawati, A. Khumaira, H. Putri, R.I. Jenie, S.M. Angraini, et al., Bioinformatics and in vitro studies reveal the importance of p53, PPARG and Notch signaling pathway in inhibition of breast cancer stem cells by hesperetin, Adv. Pharmaceut. Bull. 11 (2) (2021) 351–360, https://doi.org/10.34172/apb.2021.033.
[8] A. Hermawan, A. Khumaira, M. Ikawati, H. Putri, R.I. Jenie, S.M. Angraini, et al., Identification of key genes of hesperidin in inhibition of breast cancer stem cells by functional network analysis, Comput. Biol. Chem. 90 (2021) 107427, https://doi.org/10.1016/j.compbiolchem.2020.107427.
[9] O.S. El-Masry, B.L. Brown, P.R.M. Dobson, AMPK activation of apoptotic markers in human breast cancer cell lines with different p53 backgrounds: MCF-7, MDA-MB-231 and T47D cells, Asian Pac. J. Cancer Prev. APJCP 20 (12) (2019) 3763–3770, https://doi.org/10.31557/apjcp.2019.20.12.3763.
[10] J. Kao, K. Salari, M. Bocanegra, Y.L. Choi, L. Girard, J. Gandhi, et al., Molecular profiling of breast cancer cell lines defines relevant tumor models and provides a resource for cancer gene discovery, PLoS One 4 (7) (2009) e6146, https://doi.org/10.1371/journal.pone.0006146.
[11] J. Manuel Iglesias, I. Beloqui, F. Garcia-Garcia, O. Leis, A. Vazquez-Martin, A. Eguiara, et al., Mammosphere formation in breast carcinoma cell lines depends upon expression of E-cadherin, PLoS One 8 (10) (2013) e77281, https://doi.org/10.1371/journal.pone.0077281.
[12] J. Verigos, D. Kordias, S. Papadaki, A. Magklara, Transcriptional profiling of tumorspheres reveals TRPM4 as a novel stemness regulator in breast cancer, Biomedicines (2021), https://doi.org/10.3390/biomedicines9101368.
[13] A. Hermawan, E. Wagner, A. Roidl, Consecutive salinomycin treatment reduces doxorubicin resistance of breast tumor cells by diminishing drug efflux pump expression and activity, Oncol. Rep. 35 (3) (2016) 1732–1740, https://doi.org/10.3892/or.2015.4509.
[14] N.L. Bray, H. Pimentel, P. Melsted, L. Pachter, Near-optimal probabilistic RNA-seq quantification, Nat. Biotechnol. 34 (5) (2016) 525–527, https://doi.org/10.1038/nbt.3519.
[15] M.D. Robinson, D.J. McCarthy, G.K. Smyth, edgeR: a Bioconductor package for differential expression analysis of digital gene expression data, Bioinformatics 26 (1) (2010) 139–140, https://doi.org/10.1093/bioinformatics/btp616.
[16] S.X. Ge, D. Jung, R. Yao, ShinyGO: a graphical gene-set enrichment tool for animals and plants, Bioinformatics 36 (8) (2020) 2628–2629, https://doi.org/10.1093/bioinformatics/btz931.
[17] J. Wang, S. Vasaikar, Z. Shi, M. Greer, B. Zhang, WebGestalt 2017: a more comprehensive, powerful, flexible and interactive gene set enrichment analysis toolkit, Nucleic Acids Res. 45 (W1) (2017), https://doi.org/10.1093/nar/gkx356. W130-w7.
[18] V. Modhukur, T. Iljasenko, T. Metsalu, K. Lokk, T. Laisk-Podar, J. Vilo, MethSurv: a web tool to perform multivariable survival analysis using DNA methylation data, Epigenomics 10 (3) (2018) 277–288, https://doi.org/10.2217/epi-2017-0118.
[19] A. Hermawan, H. Putri, Characterizing excision repair cross-complementing family genes as drug resistance biomarkers in breast cancer, Beni-Suef University Journal of Basic and Applied Sciences 12 (1) (2023) 79, https://doi.org/10.1186/s43088-023-00415-3.
[20] T. Li, J. Fu, Z. Zeng, D. Cohen, J. Li, Q. Chen, et al., TIMER2.0 for analysis of tumor-infiltrating immune cells, Nucleic Acids Res. 48 (W1) (2020), https://doi.org/10.1093/nar/gkaa407. W509-w14.
[21] A. Hermawan, H. Putri, Bioinformatics analysis reveals the potential target of rosiglitazone as an antiangiogenic agent for breast cancer therapy, BMC Genomic Data 23 (1) (2022) 72, https://doi.org/10.1186/s12863-022-01086-2.
[22] J. Lamb, E.D. Crawford, D. Peck, J.W. Modell, I.C. Blat, M.J. Wrobel, et al., The Connectivity Map: using gene-expression signatures to connect small molecules, genes, and disease, Science 313 (5795) (2006) 1929–1935, https://doi.org/10.1126/science.1132939.
[23] A. Subramanian, R. Narayan, S.M. Corsello, D.D. Peck, T.E. Natoli, X. Lu, et al., A next generation connectivity Map: L1000 platform and the first 1,000,000 profiles, Cell 171 (6) (2017), https://doi.org/10.1016/j.cell.2017.10.049, 1437-52.e17.
[24] B. Chaneton, E. Gottlieb, Rocking cell metabolism: revised functions of the key glycolytic regulator PKM2 in cancer, Trends Biochem. Sci. 37 (8) (2012) 309–316, https://doi.org/10.1016/j.tibs.2012.04.003.
[25] S.-Y. Park, J.-H. Choi, J.-S. Nam, Targeting cancer stem cells in triple-negative breast cancer, Cancers 11 (7) (2019) 965.
[26] A. Terada, N. Tsuda, S. Tasaki, J. Park, H. Nasu, K. Tasaki, et al., N-myc downstream regulated gene-1 may play an important role in the prognosis of ovarian cancer, in its association with beta-catenin, Kurume Med. J. (2023), https://doi.org/10.2739/kurumemedj.MS6912010.
[27] Y. Wang, Y. Zhou, F. Tao, S. Chai, X. Xu, Y. Yang, et al., N-myc downstream regulated gene 1(NDRG1) promotes the stem-like properties of lung cancer cells through stabilized c-Myc, Cancer Lett. 401 (2017) 53–62, https://doi.org/10.1016/j.canlet.2017.04.031.
[28] Y. Feng, Y. Xiong, T. Qiao, X. Li, L. Jia, Y. Han, Lactate dehydrogenase A: a key player in carcinogenesis and potential target in cancer therapy, Cancer Med. 7 (12) (2018) 6124–6136, https://doi.org/10.1002/cam4.1820.
[29] D. Ciavardelli, C. Rossi, D. Barcaroli, S. Volpe, A. Consalvo, M. Zucchelli, et al., Breast cancer stem cells rely on fermentative glycolysis and are sensitive to 2-deoxyglucose treatment, Cell Death Dis. 5 (7) (2014) e1336–e.

[30] B.D. Johnson, W.J. Geldenhuys, L.A. Hazlehurst, The role of ERO1α in modulating cancer progression and immune escape, J Cancer Immunol (Wilmington) 2 (3) (2020) 103–115, https://doi.org/10.33696/cancerimmunol.2.023.

[31] N. Gupta, J.E. Park, W. Tse, J.K. Low, O.L. Kon, N. McCarthy, et al., ERO1α promotes hypoxic tumor progression and is associated with poor prognosis in pancreatic cancer, Oncotarget 10 (57) (2019).

[32] M. Natsuizaka, H. Kinugasa, S. Kagawa, K.A. Whelan, S. Naganuma, H. Subramanian, et al., IGFBP3 promotes esophageal cancer growth by suppressing oxidative stress in hypoxic tumor microenvironment, Am. J. Cancer Res. 4 (1) (2014) 29–41.

[33] C.G. Lee, J. Jang, H.S. Jin, A novel missense mutation in the ACTG1 gene in a family with congenital autosomal dominant deafness: a case report, Mol. Med. Rep. 17 (6) (2018) 7611–7617, https://doi.org/10.3892/mmr.2018.8837.

[34] S.T. Po'uha, M. Kavallaris, Gamma-actin is involved in regulating centrosome function and mitotic progression in cancer cells, Cell Cycle 14 (24) (2015) 3908–3919, https://doi.org/10.1080/15384101.2015.1120920.

[35] D. Studer, S. Lischer, W. Jochum, M. Ehrbar, M. Zenobi-Wong, K. Maniura-Weber, Ribosomal protein L13a as a reference gene for human bone marrow-derived mesenchymal stromal cells during expansion, adipo-, chondro-, and osteogenesis, Tissue Eng. C Methods 18 (10) (2012) 761–771, https://doi.org/10.1089/ten.tec.2012.0081.

[36] G. Oktem, O. Sercan, U. Guven, R. Uslu, A. Uysal, G. Goksel, et al., Cancer stem cell differentiation: TGFβ1 and versican may trigger molecules for the organization of tumor spheroids, Oncol. Rep. 32 (2) (2014) 641–649, https://doi.org/10.3892/or.2014.3252.

[37] M. Yasunaga, Y. Matsumura, Role of SLC6A6 in promoting the survival and multidrug resistance of colorectal cancer, Sci. Rep. 4 (1) (2014) 4852, https://doi.org/10.1038/srep04852.

[38] M. Yasunaga, Y. Matsumura, Abstract 3784: the role of the taurine transporter SLC6A6 in promoting prosurvival activity and multidrug resistance of colorectal cancer, Cancer Res. 76 (14_Supplement) (2016) 3784, https://doi.org/10.1158/1538-7445.AM2016-3784.

[39] M. Englert-Golon, M. Tokłowicz, A. Żbikowska, S. Sajdak, M. Kotwicka, M. Andrusiewicz, Differential expression of HIF1A, EPAS1, and VEGF genes in benign and malignant ovarian neoplasia, Cancers 14 (19) (2022), https://doi.org/10.3390/cancers14194899.

[40] K.L. Covello, J. Kehler, H. Yu, J.D. Gordan, A.M. Arsham, C.J. Hu, et al., HIF-2alpha regulates Oct-4: effects of hypoxia on stem cell function, embryonic development, and tumor growth, Genes Dev. 20 (5) (2006) 557–570, https://doi.org/10.1101/gad.1399906.

[41] Y. Yan, F. Liu, L. Han, L. Zhao, J. Chen, O.I. Olopade, et al., HIF-2α promotes conversion to a stem cell phenotype and induces chemoresistance in breast cancer cells by activating Wnt and Notch pathways, J. Exp. Clin. Cancer Res. 37 (1) (2018) 256, https://doi.org/10.1186/s13046-018-0925-x.

[42] M. Wagner, M. Koslowski, C. Paret, M. Schmidt, O. Türeci, U. Sahin, NCOA3 is a selective co-activator of estrogen receptor α-mediated transactivation of PLAC1 in MCF-7 breast cancer cells, BMC Cancer 13 (2013) 570, https://doi.org/10.1186/1471-2407-13-570.

[43] T.H. Truong, E.A. Benner, K.M. Hagen, N.A. Temiz, C.P. Kerkvliet, Y. Wang, et al., PELP1/SRC-3-dependent regulation of metabolic PFKFB kinases drives therapy resistant ER+ breast cancer, Oncogene 40 (25) (2021) 4384–4397.

[44] P. Pandey, B. Sliker, H.L. Peters, A. Tuli, J. Herskovitz, K. Smits, et al., Amyloid precursor protein and amyloid precursor-like protein 2 in cancer, Oncotarget 7 (15) (2016) 19430–19444, https://doi.org/10.18632/oncotarget.7103.

[45] Z. Tao, J. Huang, J. Li, Comprehensive intratumoral heterogeneity landscaping of liver hepatocellular carcinoma and discerning of APLP2 in cancer progression, Environ. Toxicol. (2023), https://doi.org/10.1002/tox.23904 n/a(n/a).

[46] E. Charafe-Jauffret, F. Monville, F. Bertucci, B. Esterni, C. Ginestier, P. Finetti, et al., Moesin expression is a marker of basal breast carcinomas, Int. J. Cancer 121 (8) (2007) 1779–1785, https://doi.org/10.1002/ijc.22923.

[47] J. Piao, S. Liu, Y. Xu, C. Wang, Z. Lin, Y. Qin, et al., Ezrin protein overexpression predicts the poor prognosis of pancreatic ductal adenocarcinomas, Exp. Mol. Pathol. 98 (1) (2015) 1–6.

[48] L. Yu, L. Zhao, H. Wu, H. Zhao, Z. Yu, M. He, et al., Moesin is an independent prognostic marker for ER-positive breast cancer, Oncol. Lett. 17 (2) (2019) 1921–1933, https://doi.org/10.3892/ol.2018.9799.

[49] S. Ahandoust, K. Li, X. Sun, B.Y. Li, H. Yokota, S. Na, Intracellular and extracellular moesins differentially regulate Src activity and β-catenin translocation to the nucleus in breast cancer cells, Biochem. Biophys. Res. Commun. 639 (2023) 62–69, https://doi.org/10.1016/j.bbrc.2022.11.075.

[50] J. Shi, L. Zhang, D. Zhou, J. Zhang, Q. Lin, W. Guan, et al., Biological function of ribosomal protein L10 on cell behavior in human epithelial ovarian cancer, J. Cancer 9 (4) (2018) 745–756, https://doi.org/10.7150/jca.21614.

[51] K. Wang, S. Chen, Y. Wu, Y. Wang, Y. Lu, Y. Sun, et al., The ufmylation modification of ribosomal protein L10 in the development of pancreatic adenocarcinoma, Cell Death Dis. 14 (6) (2023) 350, https://doi.org/10.1038/s41419-023-05877-y.

[52] A. Chatterjee, S. Gupta, The multifaceted role of glutathione S-transferases in cancer, Cancer Lett. 433 (2018) 33–42, https://doi.org/10.1016/j.canlet.2018.06.028.

[53] S. Wu, I.C. Tseng, W.C. Huang, C.W. Su, Y.H. Lai, C. Lin, et al., Establishment of an immunocompetent metastasis rat model with hepatocyte cancer stem cells, Cancers 12 (12) (2020), https://doi.org/10.3390/cancers12123721.

[54] J. Li, T. Ye, Y. Liu, L. Kong, Z. Sun, D. Liu, et al., Transcriptional activation of Gstp1 by MEK/ERK signaling confers chemo-resistance to cisplatin in lung cancer stem cells, Front. Oncol. 9 (2019) 476, https://doi.org/10.3389/fonc.2019.00476.

[55] S.Q. Wang, J.J. Chen, Y. Jiang, Z.N. Lei, Y.C. Ruan, Y. Pan, et al., Targeting GSTP1 as therapeutic strategy against lung adenocarcinoma stemness and resistance to tyrosine kinase inhibitors, Adv. Sci. 10 (7) (2023) e2205262, https://doi.org/10.1002/advs.202205262.

[56] E.C. Keeley, B. Mehrad, R.M. Strieter, CXC chemokines in cancer angiogenesis and metastases, Adv. Cancer Res. 106 (2010) 91–111, https://doi.org/10.1016/s0065-230x(10)06003-3.

[57] L.L. Marotta, V. Almendro, A. Marusyk, M. Shipitsin, J. Schemme, S.R. Walker, et al., The JAK2/STAT3 signaling pathway is required for growth of $CD44^{+}CD24^{-}$ stem cell-like breast cancer cells in human tumors, J. Clin. Invest. 121 (7) (2011) 2723–2735, https://doi.org/10.1172/jci44745.

[58] R.J. Ingham, G. Gish, T. Pawson, The Nedd4 family of E3 ubiquitin ligases: functional diversity within a common modular architecture, Oncogene 23 (11) (2004) 1972–1984, https://doi.org/10.1038/sj.onc.1207436.

[59] L. Wan, T. Liu, Z. Hong, Y. Pan, S.T. Sizemore, J. Zhang, et al., NEDD4 expression is associated with breast cancer progression and is predictive of a poor prognosis, Breast Cancer Res. 21 (1) (2019) 148, https://doi.org/10.1186/s13058-019-1236-7.

[60] S.A. Jeon, D.W. Kim, D.B. Lee, J.Y. Cho, NEDD4 plays roles in the maintenance of breast cancer stem cell characteristics, Front. Oncol. 10 (2020) 1680, https://doi.org/10.3389/fonc.2020.01680.

[61] D.J. Hazelett, S.K. Rhie, M. Gaddis, C. Yan, D.L. Lakeland, S.G. Coetzee, et al., Comprehensive functional annotation of 77 prostate cancer risk loci, PLoS Genet. 10 (1) (2014) e1004102, https://doi.org/10.1371/journal.pgen.1004102.

[62] H.A. Alzamil, J. Pawade, M.A. Fortier, A.L. Bernal, Expression of the prostaglandin F synthase AKR1B1 and the prostaglandin transporter SLCO2A1 in human fetal membranes in relation to spontaneous term and preterm labor, Front. Physiol. 5 (2014) 272, https://doi.org/10.3389/fphys.2014.00272.

[63] X. Wu, X. Li, Q. Fu, Q. Cao, X. Chen, M. Wang, et al., AKR1B1 promotes basal-like breast cancer progression by a positive feedback loop that activates the EMT program, J. Exp. Med. 214 (4) (2017) 1065–1079, https://doi.org/10.1084/jem.20160903.

[64] A. Schwab, A. Siddiqui, M.E. Vazakidou, F. Napoli, M. Böttcher, B. Menchicchi, et al., Polyol pathway links glucose metabolism to the aggressiveness of cancer cells, Cancer Res. 78 (7) (2018) 1604–1618, https://doi.org/10.1158/0008-5472.Can-17-2834.

[65] T.P. Kegelman, S.K. Das, L. Emdad, B. Hu, M.E. Menezes, P. Bhoopathi, et al., Targeting tumor invasion: the roles of MDA-9/Syntenin, Expert Opin. Ther. Targets 19 (1) (2015) 97–112, https://doi.org/10.1517/14728222.2014.959495.

[66] X. Zhao, M. Li, X. Dai, Y. Yang, Y. Peng, C. Xu, et al., Downregulation of exosomal miR-1273a increases cisplatin resistance of non-small cell lung cancer by upregulating the expression of syndecan binding protein, Oncol. Rep. 44 (5) (2020) 2165–2173, https://doi.org/10.3892/or.2020.7753.

[67] B. Qian, Z. Yao, Y. Yang, N. Li, Q. Wang, Downregulation of SDCBP inhibits cell proliferation and induces apoptosis by regulating PI3K/AKT/mTOR pathway in gastric carcinoma, Biotechnol. Appl. Biochem. 69 (1) (2022) 240–247, https://doi.org/10.1002/bab.2103.

[68] Z.Z. Shi, J.W. Zhang, S. Zheng, What we know about ST13, a co-factor of heat shock protein, or a tumor suppressor? J. Zhejiang Univ. - Sci. B 8 (3) (2007) 170–176, https://doi.org/10.1631/jzus.2007.B0170.

[69] R. Bai, Z. Shi, J.W. Zhang, D. Li, Y.L. Zhu, S. Zheng, ST13, a proliferation regulator, inhibits growth and migration of colorectal cancer cell lines, J. Zhejiang Univ. - Sci. B 13 (11) (2012) 884–893, https://doi.org/10.1631/jzus.B1200037.

[70] S. Muñoz-Galván, B. Felipe-Abrio, M. García-Carrasco, J. Domínguez-Piñol, E. Suarez-Martinez, E.M. Verdugo-Sivianes, et al., New markers for human ovarian cancer that link platinum resistance to the cancer stem cell phenotype and define new therapeutic combinations and diagnostic tools, J. Exp. Clin. Cancer Res. 38 (1) (2019) 234, https://doi.org/10.1186/s13046-019-1245-5.

[71] X. Zhu, H.H. Chen, C.Y. Gao, X.X. Zhang, J.X. Jiang, Y. Zhang, et al., Energy metabolism in cancer stem cells, World J. Stem Cell. 12 (6) (2020) 448–461, https://doi.org/10.4252/wjsc.v12.i6.448.

[72] S. Valle, S. Alcalá, L. Martin-Hijano, P. Cabezas-Sáinz, D. Navarro, E.R. Muñoz, et al., Exploiting oxidative phosphorylation to promote the stem and immunoevasive properties of pancreatic cancer stem cells, Nat. Commun. 11 (1) (2020) 5265, https://doi.org/10.1038/s41467-020-18954-z.

[73] G. Liu, Q. Luo, H. Li, Q. Liu, Y. Ju, G. Song, Increased oxidative phosphorylation is required for stemness maintenance in liver cancer stem cells from hepatocellular carcinoma cell line HCCLM3 cells, Int. J. Mol. Sci. 21 (15) (2020), https://doi.org/10.3390/ijms21155276.

[74] A. Roesch, A. Vultur, I. Bogeski, H. Wang, K.M. Zimmermann, D. Speicher, et al., Overcoming intrinsic multidrug resistance in melanoma by blocking the mitochondrial respiratory chain of slow-cycling JARID1B(high) cells, Cancer Cell 23 (6) (2013) 811–825, https://doi.org/10.1016/j.ccr.2013.05.003.

[75] O.D. Abaan, E.C. Polley, S.R. Davis, Y.J. Zhu, S. Bilke, R.L. Walker, et al., The exomes of the NCI-60 panel: a genomic resource for cancer biology and systems pharmacology, Cancer Res. 73 (14) (2013) 4372–4382, https://doi.org/10.1158/0008-5472.Can-12-3342.

[76] A. Polotskaia, G. Xiao, K. Reynoso, C. Martin, W.-G. Qiu, R.C. Hendrickson, et al., Proteome-wide analysis of mutant p53 targets in breast cancer identifies new levels of gain-of-function that influence PARP, PCNA, and MCM4, Proc. Natl. Acad. Sci. USA 112 (11) (2015) E1220–E1229, https://doi.org/10.1073/pnas.1416318112.

[77] V.V. Prabhu, J. Allen, B. Hong, S. Zhang, H. Cheng, W. El-Deiry, Therapeutic targeting of the p53 pathway in cancer stem cells, Expert Opin. Ther. Targets 16 (2012), https://doi.org/10.1517/14728222.2012.726985.

[78] A. Elwakeel, A.N. Sari, J.K. Dhanjal, H.N. Meidinna, D. Sundar, S.C. Kaul, et al., Mutant p53(l194F) harboring luminal-A breast cancer cells are refractory to apoptosis and cell cycle arrest in response to mortaparib(plus), a multimodal small molecule inhibitor, Cancers 13 (12) (2021), https://doi.org/10.3390/cancers13123043.

[79] N.T. Connell, N. Berliner, Fostamatinib for the treatment of chronic immune thrombocytopenia, Blood 133 (19) (2019) 2027–2030, https://doi.org/10.1182/blood-2018-11-852491.

[80] S.R. Park, G. Speranza, R. Piekarz, J.J. Wright, R.J. Kinders, L. Wang, et al., A multi-histology trial of fostamatinib in patients with advanced colorectal, non-small cell lung, head and neck, thyroid, and renal cell carcinomas, and pheochromocytomas, Cancer Chemother. Pharmacol. 71 (4) (2013) 981–990, https://doi.org/10.1007/s00280-013-2091-3.

[81] O. Hatton, S.L. Lambert, L.K. Phillips, M. Vaysberg, Y. Natkunam, C.O. Esquivel, et al., Syk-induced phosphatidylinositol-3-kinase activation in Epstein-Barr virus posttransplant lymphoproliferative disorder, Am. J. Transplant. 13 (4) (2013) 883–890, https://doi.org/10.1111/ajt.12137.

[82] T. Takano, K. Sada, H. Yamamura, Role of protein-tyrosine kinase syk in oxidative stress signaling in B cells, Antioxidants Redox Signal. 4 (3) (2002) 533–541, https://doi.org/10.1089/15230860260196335.

[83] M. Althubiti, Spleen tyrosine kinase inhibition modulates p53 activity, J. Cell Death 10 (2017), https://doi.org/10.1177/1179066017731564.

[84] A. Polak, E. Bialopiotrowicz, B. Krzymieniewska, J. Wozniak, M. Stojak, M. Cybulska, et al., SYK inhibition targets acute myeloid leukemia stem cells by blocking their oxidative metabolism, Cell Death Dis. 11 (11) (2020) 956, https://doi.org/10.1038/s41419-020-03156-8.

[85] W. Luo, G.L. Semenza, Emerging roles of PKM2 in cell metabolism and cancer progression, Trends Endocrinol. Metabol. 23 (11) (2012) 560–566, https://doi.org/10.1016/j.tem.2012.06.010.

[86] F. Liu, F. Ma, Y. Wang, L. Hao, H. Zeng, C. Jia, et al., PKM2 methylation by CARM1 activates aerobic glycolysis to promote tumorigenesis, Nat. Cell Biol. 19 (11) (2017) 1358–1370, https://doi.org/10.1038/ncb3630.

[87] W. Dazhi, D. Jing, R. Chunling, Z. Mi, X. Zhixuan, Elevated SLC6A6 expression drives tumorigenesis and affects clinical outcomes in gastric cancer, Biomarkers Med. 13 (2) (2019) 95–104.

[88] X. Li, Y. Li, C. Jiang, L. Chen, N. Gan, MicroRNA-144-3p inhibits tumorigenesis of oral squamous cell carcinoma by downregulating ERO1L, J. Cancer 11 (3) (2020) 759–768, https://doi.org/10.7150/jca.33267.

[89] A.A. Rawłuszko-Wieczorek, K. Horbacka, P. Krokowicz, M. Misztal, P.P. Jagodziński, Prognostic potential of DNA methylation and transcript levels of HIF1A and EPAS1 in colorectal cancer, Mol. Cancer Res. 12 (8) (2014) 1112–1127, https://doi.org/10.1158/1541-7786.MCR-14-0054.

[90] D. Li, C.Y. Xu, R.J. Cui, J.B. Tang, H. Sun, Z.K. Yang, et al., DNA methylation inhibitor, decitabine, promotes MGC803 gastric cancer cell migration and invasion via the upregulation of NEDD4-1, Mol. Med. Rep. 12 (6) (2015) 8201–8208, https://doi.org/10.3892/mmr.2015.4424.

[91] C. Deligne, K.S. Midwood, Macrophages and extracellular matrix in breast cancer: partners in crime or protective allies? Front. Oncol. 11 (2021) https://doi.org/10.3389/fonc.2021.620773.

[92] L. Wu, S. Saxena, P. Goel, D.R. Prajapati, C. Wang, R.K. Singh, Breast cancer cell-neutrophil interactions enhance neutrophil survival and pro-tumorigenic activities, Cancers 12 (10) (2020), https://doi.org/10.3390/cancers12102884.

[93] A. da Cunha, M.A. Michelin, E.F. Murta, Pattern response of dendritic cells in the tumor microenvironment and breast cancer, World J. Clin. Oncol. 5 (3) (2014) 495–502, https://doi.org/10.5306/wjco.v5.i3.495.

[94] X. Zhang, Y. Song, Y. Wu, Y. Dong, L. Lai, J. Zhang, et al., Indirubin inhibits tumor growth by antitumor angiogenesis via blocking VEGFR2-mediated JAK/STAT3 signaling in endothelial cell, Int. J. Cancer 129 (10) (2011) 2502–2511.

[95] K.H. Yan, Y.W. Lin, C.H. Hsiao, Y.C. Wen, K.H. Lin, C.C. Liu, et al., Mefloquine induces cell death in prostate cancer cells and provides a potential novel treatment strategy in vivo, Oncol. Lett. 5 (5) (2013) 1567–1571, https://doi.org/10.3892/ol.2013.1259.

[96] T. Kitabayashi, Y. Dong, T. Furuta, H. Sabit, S. Jiapaer, J. Zhang, et al., Identification of GSK3β inhibitor kenpaullone as a temozolomide enhancer against glioblastoma, Sci. Rep. 9 (1) (2019) 10049, https://doi.org/10.1038/s41598-019-46454-8.

[97] J. Wu, H. Liu, G. Zhang, L. Gu, Y. Zhang, J. Gao, et al., Antileukemia effect of ciclopirox olamine is mediated by downregulation of intracellular ferritin and inhibition β-catenin-c-Myc signaling pathway in glucocorticoid resistant T-ALL cell lines, PLoS One 11 (8) (2016) e0161509.

[98] T. Rupp, O. Pelouin, L. Genest, C. Legrand, G. Froget, V. Castagné, Therapeutic potential of Fingolimod in triple negative breast cancer preclinical models, Translational Oncology 14 (1) (2021) 100926, https://doi.org/10.1016/j.tranon.2020.100926.

[99] P.E. Goss, J.N. Ingle, J.E. Alés-Martínez, A.M. Cheung, R.T. Chlebowski, J. Wactawski-Wende, et al., Exemestane for breast-cancer prevention in postmenopausal women, N. Engl. J. Med. 364 (25) (2011) 2381–2391, https://doi.org/10.1056/NEJMoa1103507.